Czech Technical University in Prague

Faculty of Nuclear Sciences and Physical Engineering

# DIPLOMA THESIS

## Physics properties of $J/\psi$ events in testing of Inner Detector performance

Bc. Tomáš Jakoubek

Supervisor: Prom. fyz. Václav Vrba, CSc.

May 6, 2011

## Acknowledgements

I would like to thank my supervisor Václav Vrba for his invaluable help during creation of this work and for introducing me to CERN and the ATLAS experiment. My big thanks also belongs to James Catmore and Mária Smižanská for introducing me to B-physics and for many consultations and advices to my work. I am also grateful to the Institute of Physics of the Academy of Sciences of the Czech Republic for the material support and to all my colleagues, namely Michal Marčišovský, Pavel Růžička and Martin Zeman, for their valuable advice and to Jiří Popule for the organizational support during my whole work. Last but not least, I would like to thank my family and friends, especially to Tereza Liepoldová, for their support up until now.

**Prohlášení**

Prohlašuji, že jsem svou diplomovou práci vypracoval samostatně a použil jsem pouze podklady uvedené v přiloženém seznamu.

Nemám závažný důvod proti užití tohoto školního díla ve smyslu §60 Zákona č. 121/2000 Sb., o právu autorském, o právech souvisejících s právem autorským a o změně některých zákonů (autorský zákon).

**Declaration**

I declare that I wrote my diploma thesis independently and exclusively with the use of cited bibliography.

I agree with the usage of this thesis in the purport of the Act 121/2000 (Copyright Act).

Prague, May 6, 2011 Tomáš Jakoubek

*Title:* **Physics properties of $J/\psi$ events in testing of Inner Detector performance**

*Author:* Bc. Tomáš Jakoubek

*Field of study:* Nuclear Engineering

*Specialization:* Experimental Nuclear Physics

*Sort of project:* Diploma Thesis

*Supervisor:* Prom. fyz. Václav Vrba, CSc., Department of Physics, Faculty of Nuclear Sciences and Physical Engineering, Czech Technical University in Prague

*Abstract:* $J/\psi$ meson is a narrow and well known resonance with properties which allow it to be used for testing and calibration purposes of new particle detectors. This thesis is devoted to testing of the ATLAS detector at the Large Hadron Collider at CERN. For this purpose all available muon data from 7 TeV proton-proton collisions taken during the ATLAS 2010 pilot physics program were used, about 45 pb$^{-1}$ altogether. In the beginning of this thesis, fundamentals of the Standard Model can be found and the LHC accelerator and the ATLAS experiment are also briefly described. Following chapters are devoted to the analysis - it contains supporting study of primary vertices and detector tracking performance. The comparison of reconstructed $J/\psi$ data before and after Autumn 2010 reprocessing is presented towards the end of this thesis.

*Keywords:* LHC, ATLAS, $J/\psi$ , detector performance, data reprocessing

*Název práce:* **Měření vlastností J/Psi k prověření funkčnosti vnitřního detektoru experimentu ATLAS**

*Autor:* Bc. Tomáš Jakoubek

*Obor studia:* Jaderné inženýrství

*Zaměření:* Experimentální jaderná fyzika

*Druh práce:* Diplomová práce

*Vedoucí práce:* Prom. fyz. Václav Vrba, CSc., Katedra fyziky, Fakulta jaderná a fyzikálně inženýrská, České vysoké učení technické v Praze

*Abstrakt:* $J/\psi$ meson je velmi dobře proměřená rezonance. Díky svým vlastnostem je možné ji použít pro testování a kalibraci nových detektorů částic. Tato práce je zaměřena na testování detektoru ATLAS na urychlovači LHC v CERN právě pomocí této částice. K tomuto účelu byla použita veškerá data z proton-protonových srážek o energii 7 TeV nabraná detektorem ATLAS během jeho provozu v roce 2010 (celkem přibližně 45 pb$^{-1}$). V úvodních kapitolách této práce jsou nastíněny základy Standardního modelu a také stručný popis urychlovače LHC a experimentu ATLAS. Další kapitoly jsou pak věnovány samotné analýze - podpůrné studii primárních vrcholů a testování přesnosti detektoru. Na konci práce je pak porovnání rekonstruovaných $J/\psi$ dat před a po jejich přepracování na podzim roku 2010.

*Klíčová slova:* LHC, ATLAS, $J/\psi$ , výkonnost detektoru, přepracování dat

# Contents

# Chapter 1

# Introduction

Nowadays, all known matter and interactions (excluding gravity) can be described by very successful theory called **The Standard Model of Particle Physics**. This model tries to answer very fundamental questions of the nature: *from what* and *how* our world is built? One possible way how to test theories like that is to accelerate constituents of the matter (i.e. particles) to high energies and then study outcome of their collisions using complicated detectors. Such experimental complex was finished in 2008 at CERN, the world's largest laboratory for particle physics (the name is derived from the acronym for the French **C**onseil **E**uropéen pour la **R**echerche **N**ucléaire).

All detectors should be first tested and calibrated, in the case of these in **H**igh **E**nergy **P**hysics (HEP) for example by measuring some currently well known particle. This thesis is devoted to testing of the Inner Detector of the ATLAS experiment using very narrow $J/\psi$ resonance. All 2010 7 TeV data (about 45 pb$^{-1}$) were used for this purpose. Most of my work have been done in tight cooperation with the ATLAS $B$-physics group and results were presented at several ATLAS meetings held at CERN ([25], [26], [27] and [29]) and also used for further studies and measurements (e.g. [30]).

This thesis is divided into the seven chapters. Fundamentals of the Standard Model (SM) are briefly described in the first section of the chapter 2 and LHC together with its detectors in the chapter 3. Main part of this chapter it then devoted to the ATLAS experiment. Chapter 4 contains an analysis overview - some basic informations about $B$-physics *early data* analysis code, data selection and trigger settings, short introduction into the topic of primary vertices at ATLAS and fundamentals of using the unbinned maximum likelihood fit. Short section is also devoted to 2010 autumn reprocessing. Chapters 5 and 6 then contain all results of supporting vertex studies and of the Inner detector testing before and after mentioned reprocessing. Finally, summary and conclusions are presented in the chapter 7.

# Chapter 2

# Theoretical overview

## 2.1 Current state of particle physics

For the last forty years the Standard Model (SM) is the best theory describing particles and their interactions. This model postulates that there are twelve elementary particles which form all known matter in observable universe. These particles are fermions (they have half-integral spin) and can be divided into three families (see Tab. 2.1) according to their masses. In each family there are two leptons and two quarks. At present there is no explanation for this triple repetition of fermion families.

All four known interactions play their roles in the microcosmos of the particle physics, however the gravitational interaction has not yet been included into the Standard Model. The rest of interactions could be described by exchange of one or more particles. In the case of the electromagnetic interaction this particle is massless photon, while in the weak interaction, very massive $W^{\pm}$ and $Z^0$ bosons play the role. The strong interaction is mediated by massless gluons which exchange "colours" (just another quantum number) of quarks.

| | $Q$ [e] | $1^{\text{st}}$ generation | | $2^{\text{nd}}$ generation | | $3^{\text{rd}}$ generation | |
|---|---|---|---|---|---|---|---|
| Leptons | -1 | $e$ | electron | $\mu$ | muon | $\tau$ | tauon |
| | 0 | $\nu_e$ | electron neutrino | $\nu_\mu$ | muon neutrino | $\nu_\tau$ | tau neutrino |
| Quarks | $+\frac{2}{3}$ | $u$ | up | $c$ | charm | $t$ | top |
| | $-\frac{1}{3}$ | $d$ | down | $s$ | strange | $b$ | bottom |

Table 2.1: Three families of fundamental fermions. The families (generations) are structured according to increasing mass (the first generation is the lightest).

In the mathematical way, the Standard Model is constructed through use of a gauge symmetry described by the group

$$SU(3) \otimes SU(2) \otimes U(1) \tag{2.1}$$

where $SU(3)$ describes the strong interaction and the $SU(2) \otimes U(1)$ term the electroweak interaction. The electroweak symmetry group is spontaneously broken $SU(2) \otimes U(1) \rightarrow U(1)$ and as a side-effect an additional scalar field (so-called *Higgs field*) is created. This mechanism allows us to assign masses to the gauge bosons ($W^\pm$ and $Z^0$). Also some fundamental fermions *can* get their masses by interacting with this field (except neutrinos which are massless according to the Standard Model, but as we know they *have* very small mass in reality [4]).

Since 1970s, when the theory was formulated, it has passed all experimental tests and all predicted particles have been found except the Higgs boson (all SM particles are summarized in Tab. 2.2 and Tab. 2.3). Higgs boson is the quantum of the theoretical Higgs field mentioned above.

| Quark | $m$ [GeV/c$^2$] | Lepton | $m$ [MeV/c$^2$] |
|---|---|---|---|
| $d$ | $(1.7 \div 3.3) \times 10^{-3}$ | $e$ | $0.510998910 \pm 0.000000013$ |
| $u$ | $(4.1 \div 5.8) \times 10^{-3}$ | $\nu_e$ | $< 2 \times 10^{-6}$ |
| $s$ | $(101^{+29}_{-21}) \times 10^{-3}$ | $\mu$ | $105.6583668 \pm 0.0000038$ |
| $c$ | $1.27^{+0.07}_{-0.09}$ | $\nu_\mu$ | $< 0.19$ |
| $b$ | $4.19^{+0.18}_{-0.06}$ | $\tau$ | $1776.82 \pm 0.16$ |
| $t$ | $172.0 \pm 0.9 \pm 1.3$ | $\nu_\tau$ | $< 18.2$ |

Table 2.2: Fundamental fermions and their masses. Data taken from [1].

| | Particle | Spin [$\hbar$] | $Q$[\|e\|] | $m$ [GeV/c$^2$] |
|---|---|---|---|---|
| EM interaction | photon $\gamma$ | 1 | 0 | $< 1 \times 10^{-27}$ |
| Weak interaction | $W^\pm$ | 1 | $\pm 1$ | $80.399 \pm 0.023$ |
| | $Z^0$ | 1 | 0 | $91.1876 \pm 0.0021$ |
| Strong interaction | gluons $g$ | 1 | 0 | 0 |
| Higgs field | $H$ (?) | 0 | 0 | $> 114.4$ |

Table 2.3: Basic properties of Standard Model bosons. The Higgs particle (or particles) has not yet been observed. Data taken from [1].

Since the Higgs boson is so crucial in the Standard Model, much of today's research in high energy physics focuses on the search for this particle. Unfortunately, the Standard Model does not predict its mass. The lower limit is 114.4 GeV, which is the combined result from four **L**arge **E**lectron-**P**ositron Collider (LEP) experiments. However, the LEP collaboration was unable to see any Higgs signal. The same situation seems to be at Tevatron, the previous[1] largest particle accelerator, although its energy was 1.96 TeV.

Despite its durability, the Standard Model is very unsatisfactory theory. In addition to still unobserved Higgs boson there are many other problems and questions, for example:

- The theory contains 19 free parameters - numbers that cannot be derived from fundamental physics, but have to be measured and then fed into the model.
- The gravitational interaction has not yet been included into the model.
- There is no explanation for the triple repetition of fermion families (see above).
- Are all these fundamental fermions really *fundamental*?
- Where the neutrino masses come from?
- Why there is so big imbalance between matter and anti-matter in the observed universe?

These are reasons why some scientists believe that the Standard Model cannot tell the whole story. They are searching for extensions to the electroweak theory that make it more predictive. One approach is a generalization of this theory, called supersymmetry. It postulates a fermion-boson symmetry, according to which new fermion (boson) partners are postulated for all known fundamental bosons (fermions). These superpartners should be heavier than the known elementary particles, but the accurate predictions of the the superpartner masses do not exist. However, there are some distinct arguments that make qualitative predictions of the masses - a typical superpartner mass should be in the range of $100 \div 1000$ GeV [2], [3], which falls in the energy range of the **L**arge **H**adron **C**ollider (LHC), the current largest particle accelerator. It is designed for the center of mass energy of 14 TeV in proton-proton (*pp*) collisions. Due to the large energy, the LHC should be a Higgs factory and thus has a big potential to discover it (if it in fact exists). In addition to Higgs and supersymmetry, LHC and its experiments have many other goals, some of them connected to the SM problems and questions mentioned above. This accelerator will be briefly described in the

[1]Until March 30, 2010.

next chapter, the major part will be then devoted to the ATLAS experiment, one of the general-purpose LHC detectors.

## 2.2 $B$-physics

$B$-physics is a common name for the field of study concerning beauty particles, i.e. particles containing $b$-quark, and related processes.

Since its discovery, the $b$-quark brought us two big surprises. The first was the unexpectedly large lifetime. The second one was that the mass difference between the two mass eigenstates of the $B_d$ meson system is $\sim 100$ times larger than the similar mass difference in the neutral $K^0$ meson system.

One of the main goals of $B$-physics is to study the structure of the quark mixing and its role in $CP$-violation[2]. It can be very naturally accommodated in the Standard Model through the CKM[3] matrix and all the currently observed $CP$-violation phenomena in particle physics are in full agreement with the Standard Model calculations. However, there are still some reasons to speculate about $CP$-violation generated by physics beyond the Standard Model. Since $CP$-violation is expected in many $B$ meson decay modes and the Standard Model can make precise predictions for some of those decay modes, the $B$ meson system appears to be a very attractive place to look for evidence for physics beyond the Standard Model.

The goal of $B$-physics in the LHC era is to determine the CKM parameters in a model-independent way and to isolate the effect of New Physics so that its characteristics could be identified. This calls for an experiment capable of studying $CP$-violation with both $B^0$ and $B_s^0$ systems decaying into various final states including those with only hadrons, with high statistics. The production cross section of the $b\bar{b}$ quark pairs at the LHC energy is estimated to be $\sim 500\ \mu$b; far larger than at any other machines [6]. Thus, LHC appears to be a very promising place to perform high precision $CP$-violation measurements in the $B$-meson decays.

Besides $CP$-violation, there are many other fields of study - for example by measuring production cross-sections of beauty and charm hadrons and of the heavy-flavour quarkonia, $J/\psi$ and $\Upsilon$, sensitive tests of QCD predictions of production in $pp$ collisions could be provided. The first mentioned meson - $J/\psi$ - could be also used for testing and calibrating the detector since it is well known and narrow resonance.

[2]Violation of the $CP$ symmetry, i.e. of the product of two symmetries: **C**harge conjugation symmetry and **P**arity symmetry. The first one transforms a particle into its antiparticle and the second one creates the mirror image of a physical system.

[3]In the Standard Model, $CP$-violation is naturally introduced by the $3 \times 3$ complex Cabibbo-Kobayashi-Maskawa (CKM) quark mixing matrix. See e.g. [6] for more informations.

### 2.2.1 $J/\psi$ meson

This bound state of a charm quark and a charm anti-quark was found independently by two research groups, one at the Stanford Linear Accelerator Center (headed by Burton Richter) and one at the Brookhaven National Laboratory (headed by Samuel Ting) in 1974. The discovery of $J/\psi$ provided support for the theory that there existed a fourth quark in addition to those predicted by early quark models (i.e., the up, down, and strange quarks). Basic properties of the $J/\psi$ meson are summarized in Tab. 2.4 and some examples of the $J/\psi$ production mechanisms are shown in Fig. 2.1.

| | |
|---|---|
| Mass | $(3096.916 \pm 0.011)$ MeV |
| Full width | $(92.9 \pm 2.8)$ keV |
| Branching ratios of main decay modes | |
| hadrons | $(87.7 \pm 0.5) \times 10^{-2}$ |
| virtual $\gamma \to$ hadrons | $(13.50 \pm 0.30) \times 10^{-2}$ |
| $ggg$ | $(64.1 \pm 1.0) \times 10^{-2}$ |
| $\gamma gg$ | $(8.8 \pm 0.5) \times 10^{-2}$ |
| $e^+e^-$ | $(5.94 \pm 0.06) \times 10^{-2}$ |
| $\mu^+\mu^-$ | $(5.93 \pm 0.06) \times 10^{-2}$ |

Table 2.4: Basic properties of the $J/\psi$ meson. Data taken from [1].

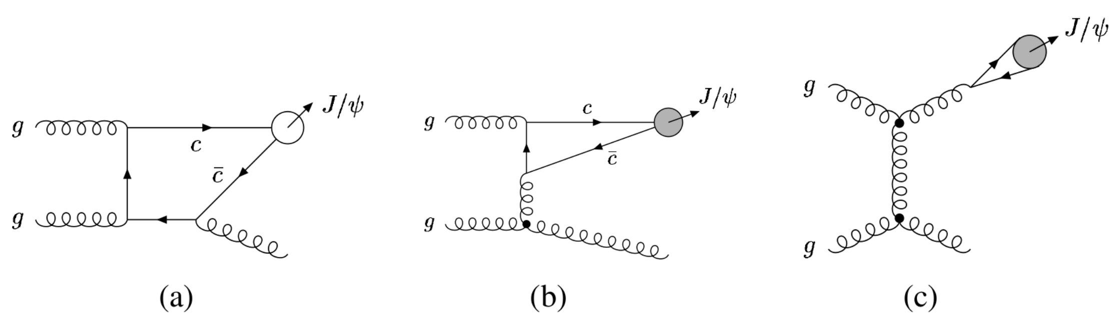


Figure 2.1: Some example Feynman diagrams for the singlet and octet $J/\psi$ production mechanism: (a) The leading colour-singlet subprocess. In the accessible range of transverse momenta of $J/\psi$ its contribution is expected to be small. (b) The dominant subprocess at the lower $p_T$ - both singlet and octet $c\bar{c}$ states with various quantum numbers contribute to the production through $\chi_{cJ} \to J/\psi + \gamma$ decays and/or soft gluon emission. (c) The gluon fragmentation subprocess becomes increasingly dominant at high $p_T$. Figure from [12].

An introduction to various topics in heavy-flavour physics, the theory and phenomenology of heavy-quark symmetry, exclusive weak decays of $B$ mesons, inclusive decay rates, and some rare $B$ decays can be found for example in [5] or [6].

# Chapter 3

# The ATLAS experiment

The world's most powerful accelerator, the **L**arge **H**adron **C**ollider (LHC), was finished at CERN in 2008. It is a synchrotron designed for *pp* collisions with the center of mass energy of 14 TeV and also heavy ion (nuclei of lead, $Pb^{82+}$) collisions with energy of 1150 TeV. In addition to the greatest energy, the LHC also aims for the greatest luminosity. That should reach $10^{34}$ cm$^{-2} \cdot$ s$^{-1}$ and 100 fb$^{-1}$ of the integrated luminosity per year. To achieve these values, the beams have to have the corresponding density - in each beam there will be 2808 bunches of $1.15 \times 10^{11}$ particles. Bunches will be separated by 25 ns, thus the bunch crossing rate will be 40 MHz. Another interesting fact is the pressure in the beampipes ($10^{-13}$ atm) and the magnetic field (about 8.33 T) produced by superconducting magnets, which are cooled to remarkable temperature of 1.9 K. For more information see [8].

To measure the outcome of this powerful accelerator, there are four major and some smaller experiments along the course of the LHC ring (locations of major experiments are on the Fig. 3.1):

**ATLAS** (**A** **T**oroidal **L**HC **A**pparatu**S**) is a general-purpose detector designed to cover the widest possible range of physics at the LHC. The main goals of the ATLAS experiment are the search for the Higgs boson, the study of $CP$-violation, the precise measurement of mass of heavy particles, the search for appropriate superparticles or extra dimensions and for particles that could make up *dark matter* - a (still hypothetical) form of matter that does not emit or reflect enough electromagnetic radiation to be observed directly, but whose presence can be inferred from gravitational effects. ATLAS is the largest collider detector ever constructed. Its parts will be described in following sections.

**CMS** (**C**ompact **M**uon **S**olenoid) is also a general-purpose detector, optimized for tracking muons. The word "compact" means that is smaller than the ATLAS detector. CMS and ATLAS have the same physics goals, but different technical solutions and design. That means they can independently confirm

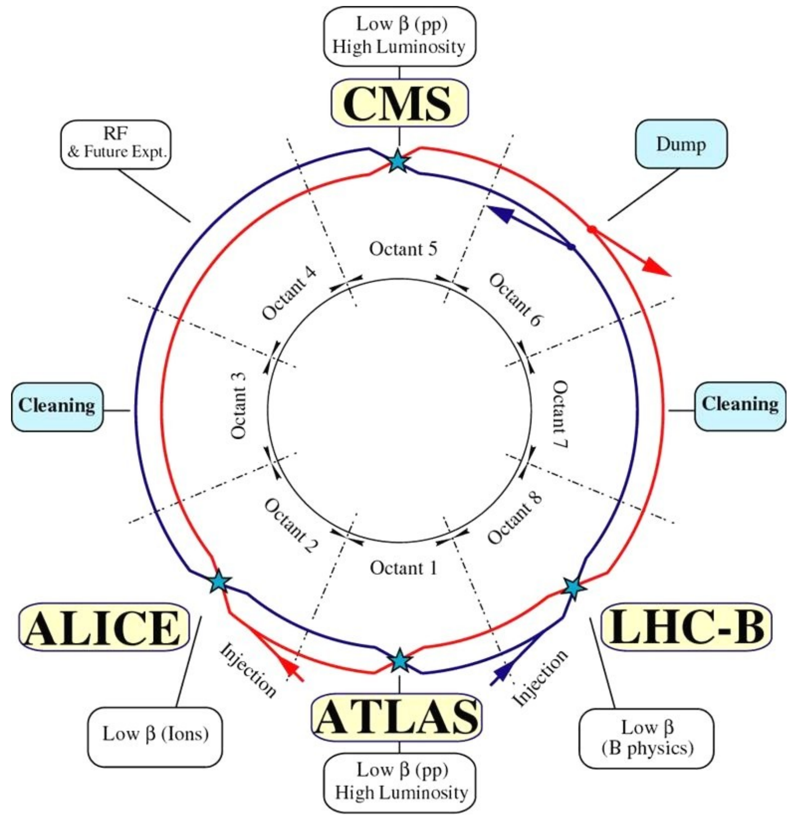


Figure 3.1: The scheme of the LHC and locations of four major experiments. Two smaller experiments are placed near ATLAS (LHCf) and CMS (TOTEM). Figure from [7].

the results flowing from the same physical phenomena and reduce systematic and random errors. Moreover, CMS also tries to study heavy ion collisions and the quark-gluon plasma (QGP).

**ALICE** (**A** **L**arge **I**on **C**ollider **E**xperiment) is a detector specialized in analysing heavy ions collisions and it studies the properties of QGP.

**LHCb** (**L**arge **H**adron **C**ollider **b**eauty) specializes in the study of the slight asymmetry between matter and antimatter present in interactions of $B$-particles and thus help us to understand why the Universe we live in appears to be composed almost entirely of matter, but no antimatter.

**LHCf** (**L**arge **H**adron **C**ollider **f**orward) is a small experiment designed for astroparticle physics. It measures particles produced very close to the direction of the beams in the $pp$ collisions. The motivation is to test models used to estimate the primary energy of the ultra high-energy cosmic rays.

**TOTEM** (**TOT**al **E**lastic and diffractive cross section **M**easurement) measures the effective size or "cross-section" of the proton at LHC, studies forward particles to focus on physics that is not accessible to the general-purpose experiments and also independently monitors the luminosity of the LHC.

As mentioned above, ATLAS has really ambitious goals, so it has to be very complex, has to have high resolution tracking and precise calorimetric energy measurements. The detector consists of four major components: the *Inner Detector* which measures tracks of all charged particles, the *calorimeter* which measures the energies carried by the particles, the *muon spectrometer* which identifies and measures muons and the *magnet system*. Some of them will be described below. The schematic view of the whole detector with all mentioned components is on the Fig. 3.2.

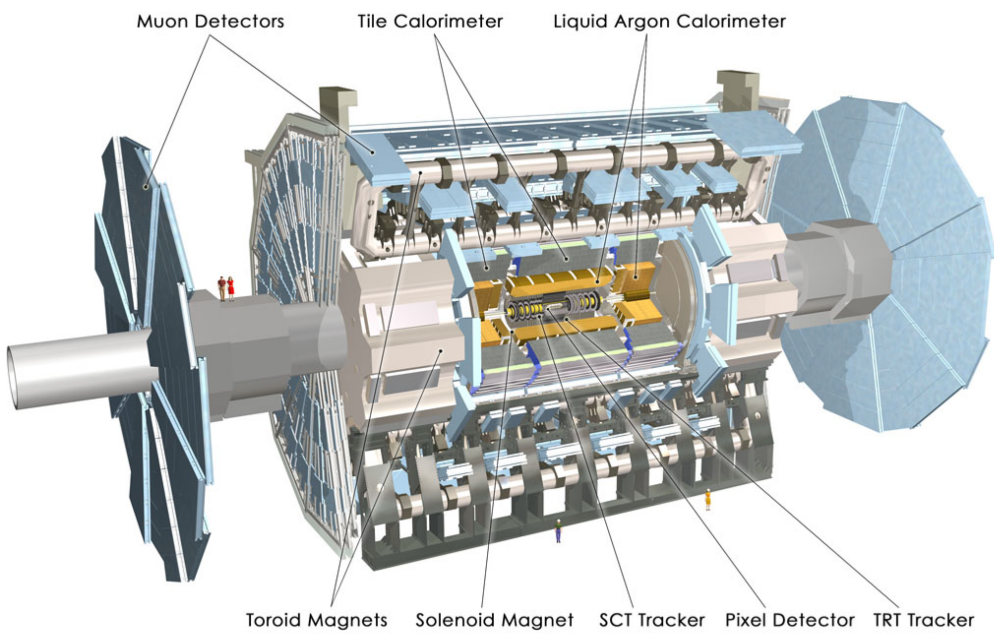


Figure 3.2: The schematic view of the ATLAS detector. Figure from [9].

## 3.1 Coordinate system

Throughout this thesis, the standard ATLAS coordinate system is employed. It is a right-handed system with the $x$-axis pointing to the centre of the LHC ring, the $z$-axis following the beam direction and the $y$-axis going upwards. In Point 1, positive $z$ points towards Point 8.

The azimuthal angle $\phi = 0$ corresponds to the positive $x$-axis and $\phi$ increases clock-wise looking into the positive $z$ direction. $\phi$ is measured in the range $\langle -\pi, +\pi)$. The polar angle $\theta$ is measured from the positive $z$ axis. Pseudorapidity $\eta$ is defined by

$$\eta = -\log\left(\tan\frac{\theta}{2}\right) \tag{3.1}$$

Transverse momentum $p_T$ is the momentum perpendicular to the LHC beam axis. Transverse impact parameter $d_0$ is defined as the distance of the closest approach of helix to beampipe and longitudinal impact parameter $z_0$ as the $z$ value at the point of closest approach. The convention for the sign of $d_0$ is the following: may $\phi$ denote the azimuthal angle to the perigee position and $\phi_0$ the azimuthal angle of the momentum in the perigee. The sign of $d_0$ is then defined as positive, if $\phi - \phi_0 = \frac{\pi}{2} + n \cdot 2 \cdot \pi$, where $n \in Z_0$. Fig. 3.3 shows these parameters, split into transverse parameters ($x$-$y$ plane) and longitudinal parameters ($r$-$z$ view) [13].

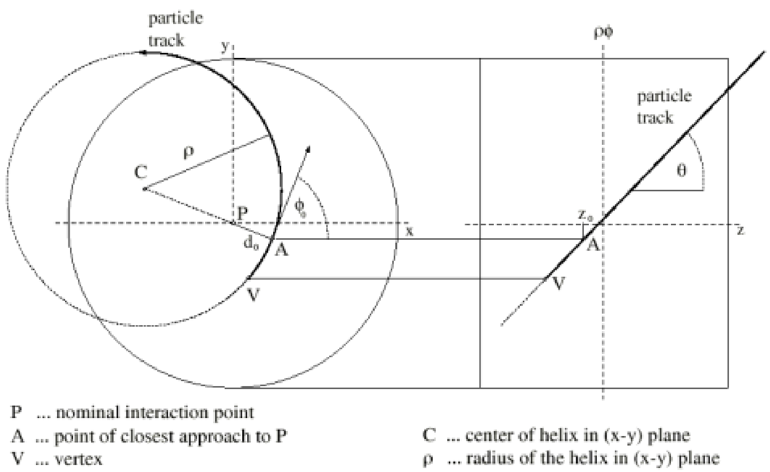


Figure 3.3: The drawing of main track parameters used in the ATLAS detector. Figure from [13].

## 3.2 Tracking system

Precise ATLAS tracking is done by the Inner Detector (ID), which combines high-resolution detectors at the inner part with continuous straws of Transition Radiation Tracker (see below) at the outer part, all contained in the central solenoid which provides a nominal magnetic field of 2 T. The outer radius is 1.15 m and the total length is 7 m. The Inner Detector should give us detailed tracking information about the first part of the particle's trajectory - it covers a pseudorapidity range up to $|\eta| < 2.5$. The momentum and vertex resolution requirements from physics call for high-precision measurements to be made with fine-granularity detectors, given the very large track density. Semiconductor tracking detectors, using pixel and silicon microstrip technologies offer these features. As shown on the Fig. 3.4, the Inner Detector consists of three subsystems which will be described below. All relevant dimensions are shown on the Fig. 3.5.

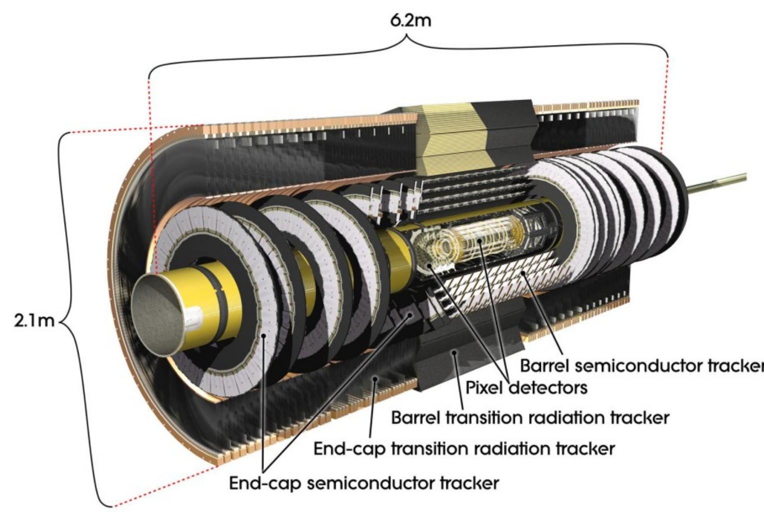


Figure 3.4: The schematic view of the ATLAS Inner Detector. Figure from [9].

### 3.2.1 The Pixel detector

The Pixel detector is the innermost part of the Inner Detector. It provides a very high-granularity, high-precision set of measurements as close to the interaction point as possible. The system determines the impact parameter resolution and the ability of the Inner Detector to find short-lived particles such as $B$ hadrons and $\tau$ leptons.

The detector consists of three barrels and three disks of each end-cap. The barrel layers are made of identical staves inclined with azimuthal angle of 20° and each stave is composed of 13 pixel modules. One end-cap disk is made of 8 sectors, with 6 modules in each sector (disk modules are identical to the barrel modules, except the connecting cables). Altogether there are 1744 pixel modules.

The module dimensions are 16.4 mm $\times$ 60.8 mm and on each there are 16 front-end chips and one module control chip. One front-end chip contains 16 columns of 400 $\mu$m and 2 columns of 600 $\mu$m (so-called *long*) pixels, and 160 normal plus 4 ganged rows of 50 $\mu$m pixels. Thus, the short side of the module has a 50 $\mu$m pitch and the long side has a 400 $\mu$m pitch with the only exception of long and ganged pixels. The intrinsic accuracies in the barrel are 10 $\mu$m (R-$\phi$) and 115 $\mu$m (z) and in the disks are 10 $\mu$m (R-$\phi$) and 115 $\mu$m (R). The Pixel detector has approximately 80.4 million readout channels [11], [12].

### 3.2.2 Semiconductor Tracker

The second part of the Inner Detector is the **S**emi**C**onductor **T**racker (SCT). Its design is very similarly to the Pixel detector, but instead of pixels it uses the silicon strips for detection.

The barrel part of the detector uses eight layers of silicon microstrip sensors to provide precision position measurement. The modules are mounted on carbon-fibre cylinders which carry the cooling system. The end-cap modules are mounted in up to three rings onto nine wheels, which are interconnected by a space-frame. Each silicon sensor is 6.36 cm $\times$ 6.40 cm with 768 readout strips of 80 $\mu$m pitch. The intrinsic accuracies per module in the barrel are 17 $\mu$m (R-$\phi$) and 580 $\mu$m (z) and in the disks are 17 $\mu$m (R-$\phi$) and 580 $\mu$m (R). The total number of readout channels in the SCT is approximately 6.3 million [11], [12].

### 3.2.3 Transition Radiation Tracker

The last part of the Inner Detector is the **T**ransition **R**adiation **T**racker (TRT), which covers a pseudorapidity range up to $|\eta| < 2.0$. It is based on the use of straw detectors, which can operate at the expected high rates due to their small diameter. This system detects the transition radiation photons which were created by passing particles.

The barrel contains about 50 000 straws, each divided in two at the center, and the end-caps contain 320 000 radial straws. Each straw is 4 mm in diameter and equipped with a 30 $\mu$m diameter gold-plated wire. Because of a large number of the straws, TRT produces about 30 hits for each track.

The TRT only provides R-$\phi$ information, for which it has an intrinsic accuracy of 130 $\mu$m per straw. In the barrel region, the straws are parallel to the beam axis and are 144 cm long, with their wires divided into two halves, approximately at $\eta = 0$. In the end-cap region, the 37 cm long straws are arranged radially in wheels. The total number of TRT readout channels is approximately 351,000 [11], [12].

## 3.3 Muon detection

The only charged particles that can travel through all of the calorimeter material placed around the Inner Detector are muons. They lose energy almost entirely by the formation of electron-ion pairs along their path, and for a substance like

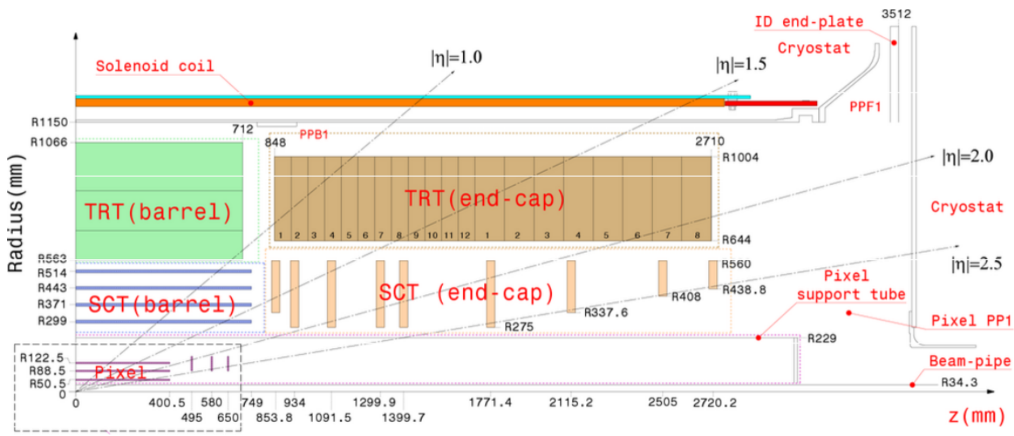


Figure 3.5: The plan view of a quarter-section of the ATLAS Inner Detector showing each of the major elements with its active dimensions. Figure from [14].

steel, this amounts to an energy loss of about 1.57 MeV per millimetre of path. Thus muons with energy above 5 GeV will penetrate about 7.8 m of steel, whereas hadrons of almost any energy are completely absorbed in about 2 m of steel. Therefore it is nearly certain that energetic particles seen outside the hadron calorimeter are muons.

The Muon Spectrometer (MS) covers the pseudorapidity range $|\eta| < 2.7$ and allows identification of muons with momentum above 3 GeV/c and precise determination of $p_T$ up to about 1 TeV/c. To measure it, superconducting coils (see Fig. 3.6) provide a toroidal magnetic field whose integral varies significantly as a function of both $\eta$ and $\phi$. The integrated bending strength is roughly constant as a function of $\eta$ except for a significant drop in the transition between the barrel and end-cap toroid coils ($1.4 \lesssim |\eta| \lesssim 1.6$).

In the barrel region ($|\eta| < 1$), muons are measured in three widely-separated layers of chambers consisting of precise **M**onitored **D**rift **T**ubes (MDTs) and fast **R**esistive **P**late **C**hambers (RPCs) used for triggering. MDTs stations includes multiple closely-packed layers measuring the $\eta$ coordinate (the direction in which most of the magnetic field deflection occurs) and provide these measurements everywhere except in the high $\eta$ region ($|\eta| > 2.0$, the end-cap regions) of the innermost station. There **C**athode **S**trip **C**hambers (CSCs) are used for precise measuring and **T**hin **G**ap **C**hambers (TGCs) for triggering. The MDTs measurement precision in each layer is typically better than 100 $\mu$m, the CSCs additionally provide a rough (1 cm) measurement of the $\phi$ coordinate [11], [12].

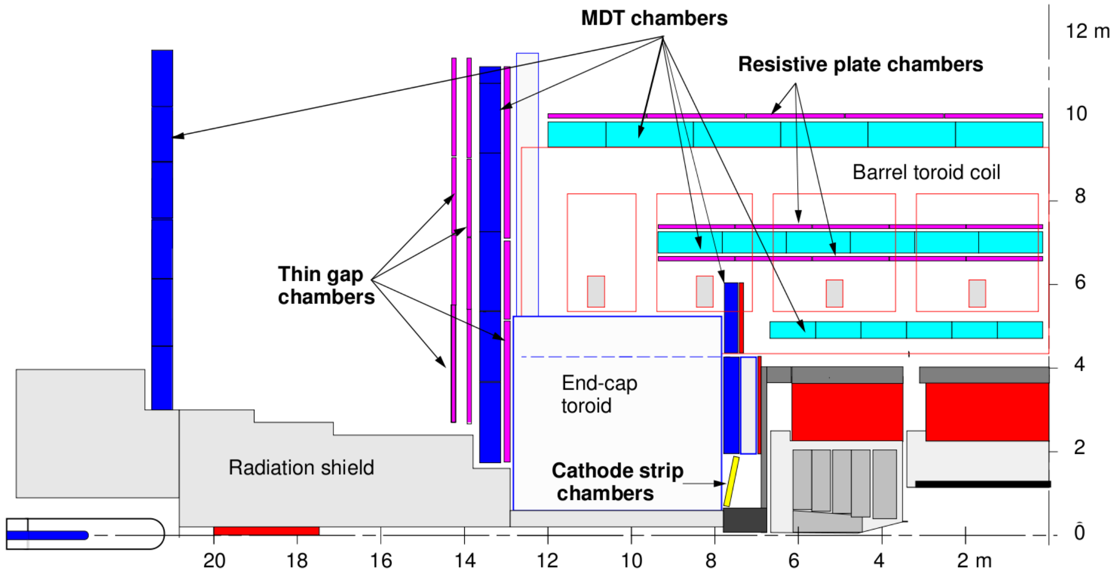


Figure 3.6: The plan view of a quarter-section of the ATLAS Muon System showing each of the major elements with its active dimensions. Figure from [12].

### 3.3.1 Muon reconstruction

There are several strategies for identifying and reconstructing muons in the ATLAS experiment (see Fig. 3.7). And for each strategy, two algorithms (STACO [15] or Muid [16]) could be employed.

During reconstruction of so called **Standalone muons** (Fig. 3.7a), algorithms first build track segments in each of the three MS stations and then link the segments to form tracks (extrapolating these to the beam line). The extrapolation must account for both multiple scattering and energy loss in the calorimeter.

**Combined muons** (Fig. 3.7c) are found by matching standalone muons to nearby ID tracks and then combining the measurements from the two systems. STACO does a statistical combination of the inner (ID) and outer (MS) track vectors to obtain the combined track vector. Muid does a partial refit: it does not directly use the measurements from the inner track, but starts from the inner track vector and covariance matrix and adds the measurements from the outer track. The fit accounts for the material (multiple scattering and ionization energy loss) and magnetic field in the calorimeter and muon spectrometer.

**Tagged muons** (Fig. 3.7d and 3.7e) are found by extrapolating inner detector tracks to the spectrometer detectors and searching for nearby hits. Calorimeter tagging algorithms are also being developed to tag inner detector tracks using the presence of a minimum ionizing signal in calorimeter cells [12].

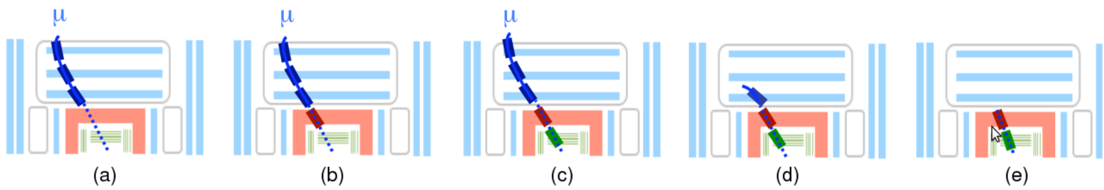


Figure 3.7: Reconstructed muon types: (a) Standalone muons (MS only), (b) Standalone muons corrected for the energy loss in the calorimeters (MS and calorimeter), (c) Combined muons (ID, MS and calorimeter), (d) Segment-Tagged Muons (ID, calorimeter and at least one MS segment), (e) Calo-Tagged Muons (ID and calorimeter). Figure from [12].

## 3.4 Trigger system

The main task of the ATLAS trigger is not easy: it has to reduce a flux of information from $10^9$ Hz to 200 Hz, but it must not to discard interesting events (for example, a Standard Model Higgs particle with a mass of 120 MeV, decaying into two photons, is expected to occur at a rate of $10^{-13}$ of the interaction rate... the proverbial pin in the haystack).

The triggering process is divided into three steps. The first step (LVL1 trigger) is implemented as a hardware trigger, the second and third steps (LVL2 trigger and Event Filter) are software triggers and are usually referred to as the ATLAS **H**igh **L**evel **T**rigger (HLT). The scheme of the ATLAS trigger is shown on the Fig. 3.8.

LVL1 trigger reduces the initial 40 MHz to less than 75 kHz in less than 2.5 $\mu$s. It looks for regions of potentially interesting activity in the Calorimeters and the Muon Spectrometer (RPC for $|\eta| < 1$ and TGC for $1 < |\eta| < 2.4$) that may correspond to candidates for high $p_T$ leptons, hadrons or jets. This is known as **R**egion **o**f **I**nterest (RoI) concept (see Fig. 3.9).

The LVL2 selection is largely based on RoI information of the LVL1 trigger and uses fine-grained data from the detector for a local analysis of the LVL1 candidate. The LVL2 trigger reduces the rate to approx. 1 kHz and its latency is about 10 ms.

Event Filter further reduces the rate to frequency of about 200 Hz (latency is approx. 1 s). The RAW data of the full event are passed to the Event Builder, which collects the pieces of information connected to this event and put them into a single memory. The size of each event saved at the permanent data storage is about 1.5 MB.

### 3.4.1 The muon trigger

$B$-physics programme of the ATLAS experiment includes the study of production cross sections, searches for rare $b$ decays and measurements of $CP$-violation ef-

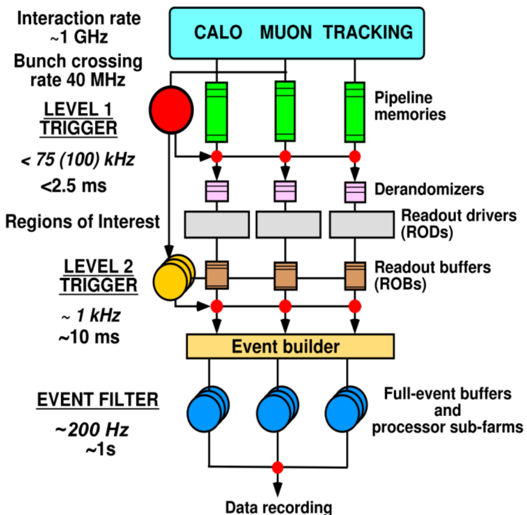


Figure 3.8: The scheme of the ATLAS trigger. Figure from [17].

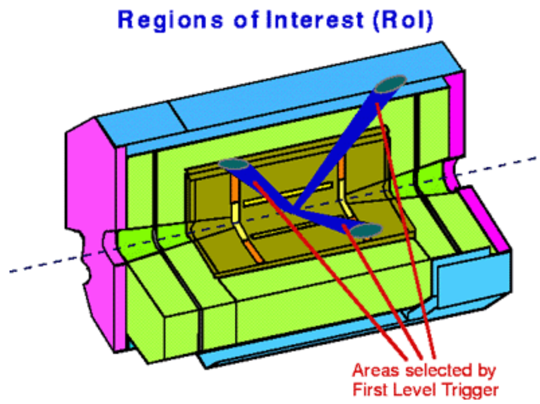


Figure 3.9: The example of Regions of interest selected by LVL1 trigger. These are used by the further trigger levels. Figure from [9].

fects. These studies make use of the large $b\bar{b}$ production cross section at the LHC where $b\bar{b}$ pairs are abundant in the low $p_T$ region. On the other hand, one must extract signals from amongst the large QCD background, mostly composed of light quarks. For this purpose, one of the main channels for $B$-physics study involves decay channels with one or more muons in the final state, especially the channel $J/\psi \rightarrow \mu^+\mu^-$. Although branching ratios for $J/\psi$ dilepton decay channels are almost the same (see Tab. 3.1), the muon one is more promising on the ATLAS experiment, since muons can be measured with better precision than electrons there. Thus basically all triggers in current $B$-physics analysis are muon triggers.

| Decay channel | Branching ratio |
|---|---|
| $J/\psi \rightarrow e^+e^-$ | $(5.94 \pm 0.06) \times 10^{-2}$ |
| $J/\psi \rightarrow \mu^+\mu^-$ | $(5.93 \pm 0.06) \times 10^{-2}$ |

Table 3.1: Branching ratios for $J/\psi$ dilepton decay channels. Data taken from [1].

### The level-1 muon trigger

The level-1 muon trigger is based on dedicated fast detectors: RPC in the barrel and the TGC in the end-caps. The basic principle of the algorithm is to require a coincidence of hits in the different muon chamber layers within a predefined angular region from the interaction point through the detector. The trigger in both the barrel and the end-cap regions is based on three trigger stations at different distances from the interaction point.

### The level-2 single-muon trigger

Level-2 muon trigger confirms muon candidates flagged by the level-1 and gives more precise track parameters for the muon candidate. The level-2 muon selection is performed in two stages. In the first stage an algorithm starts from a level-1 muon RoI and reconstructs the muon in the spectrometer, using the more precise MDT to perform a new $p_T$ estimate for the muon candidate and creating a new trigger element. In the next stage, ID tracks from region of the muon candidate together with this candidate are passed to the next algorithm, which matches an ID track with the trigger element from the muon spectrometer and refines the $p_T$ estimate.

### The level-2 di-muon triggers

There are two approaches at level-2 for selecting di-muon events from a resonance such as $J/\psi$ . The first approach is to start from a di-muon trigger at level-1 which produces two muon RoIs. Reconstruction of a muon is confirmed separately in each RoI and the two muons are subsequently combined to form a resonance and to apply a mass cut. This is usually referred as the “topological di-muon trigger”. The second approach is to start with a level-1 single muon trigger and search for two muons in a wider $\eta$ and $\phi$ region. Since this method does not explicitly require the second muon at level-1, it has an advantage for reconstructing $J/\psi$ at low-$p_T$. This is implemented in the “TrigDiMuMuon” algorithm. The two approaches are illustrated in Fig. 3.10.

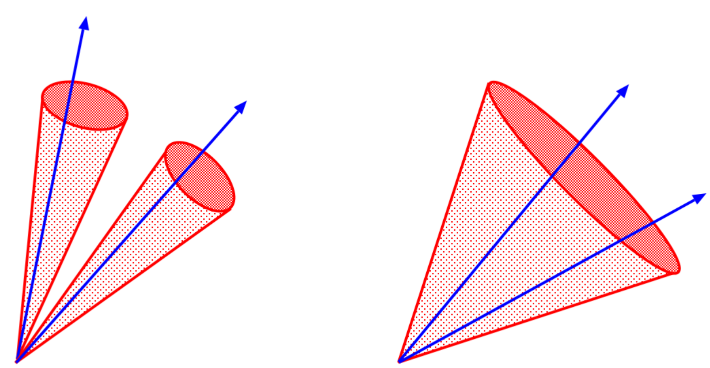

Figure 3.10: Schematic picture of RoI based di-muon trigger, using two RoIs (left) and seeded by a single muon RoI (right). Figure from [12].

Summarized information about the ATLAS detector and all its systems together with physics programme can be found in [11] and [12].

## 3.5 The ATLAS Offline Software

### 3.5.1 The ATHENA framework

There is a need for a common framework for physicists plug-in their ideas. In the case of the ATLAS experiment, that framework is called **Athena**. Athena is based on C++ and Python and it is an enhanced version of the Gaudi framework that was originally developed by the LHCb experiment, but now it is a common ATLAS–LHCb project. Athena and Gaudi are concrete realizations of a component-based architecture (also called Gaudi) which was designed for a wide range of physics data-processing applications. Apart from common data types, methods and functions, Athena also contains a central software repository for all algorithms. Everything can be managed by using the **C**onfiguration **M**anagement **T**ool (CMT). The Athena documentation is based on TWiki [18]; one can found there many manuals, tutorials and user experiences.

Athena uses a unified hierarchy of data types. Each of them has some advantages and disadvantages (mainly the size) [19]:

**RAW data** are events as output by the Event Filter (see section 3.4) for reconstruction. They can be also used for trigger analysis. The event size should be about 1.6 MB, arriving at an output rate of 200 Hz.

**ESD** (**E**vent **S**ummary **D**ata) refers to event data written as the output of the reconstruction process. Its content is intended to make access to RAW data unnecessary for most physics applications other than for some calibration or re-reconstruction. The size of one event in ESD is about 500 kB

**AOD** (**A**nalysis **O**bject **D**ata) is a reduced event representation, derived from ESD, suitable for analysis. It contains physics objects and other elements of analysis interest. The target size is 150 kB per event.

**TAG data** are event-level metadata - thumbnail information about events to support efficient identification and selection of events of interest to a given analysis. The assumed average size is 1 kB per event.

**DPD** (**D**erived **P**hysics **D**ata) is an n-tuple-style representation of event data for end-user analysis and histogramming. In general people in different groups make different DPD files using the same input data.

It is good to mention that simulated data are often larger, in part because they usually retain Monte Carlo “truth” information.

However, Athena is not only the reconstruction and analysis algorithms for the real ATLAS data. It contains also all other software needed for the HEP computing. All these software together form a software chain which is needed to produce the simulated AOD file on which analysis can be performed.

Until the analysis phase, everything could be done automatically by software and all data are same for the whole collaboration. However in the phase of analysis, physicists with their intuition are needed. They should interpret the reconstruction results (for example compute invariant mass of the muon pair in the $Z \rightarrow \mu\mu$ events) and try to find what actually happened. For this purpose, every physicist can write his analysis algorithm. In such algorithm, one can use some of various Athena packages (provided by CMT, see [18] for more information) or write a new one on is own. The output of this analysis part can be then visualized in some software - pictures are more comprehensible for human mind than numbers. In the case of the ATLAS experiment there are two ways to do this: The first one is to plot a histogram. The most used programme is **ROOT** (see next subsection), which is very popular in HEP community. The second way is to use an event viewer. In the case of ATLAS, there are two possibilities: **Atlantis** and **VP1** (**V**irtual **P**oint **1**). Both can be used for the visual investigation and the understanding of the physics of complete events, or as a tool for creating pictures and animations for publications and presentations. Atlantis is a stand-alone Java application, which uses simplified detector geometry and provides 2D pictures of some specific event. As an input, it uses so-called *jiveXML* files that have to be produced during reconstruction or analysis on top of the standard output. On the other hand, VP1 runs out of the Athena framework and thus provides direct access to the same data and algorithms. Another advantage of VP1 is e.g. 3D view with direct mouse/keyboard rotation. More information and documentation can be found on the websites [23] and [24].

### 3.5.2 ROOT

It is an object-oriented framework and is also written in C++. Both frameworks, ROOT and Athena, are well connected, but in general, they are absolutely independent. ROOT can be used in an interactive mode (writing the C++ statements on the CINT command line) or it is possible to write a script and then execute it. It is very powerful and universal software, which can be used for example for histogramming and graphing to visualize and analyse distributions and functions, curve fitting (regression analysis) and minimization of residuals, statistics and data analysis, matrix algebra, but also for drawing the Feynman diagrams or 3D visualization of the detector. Many examples, documentation and downloadable binaries/source codes can be found on the ROOT website [20].

### 3.5.3 RooFit

The RooFit is a library which provides a toolkit for modelling the expected distribution of events in a physics analysis. Models can be used to perform unbinned maximum likelihood fits, produce plots and generate "toy Monte Carlo" samples for various studies. The RooFit tools are integrated with the ROOT environment. The core functionality of RooFit is to enable the modelling of event data distributions, where each event is a discrete occurrence in time, and has one or more measured observables associated with it. The natural modelling language for such distributions are probability density functions (PDFs). The library contains basic PDFs such as Gaussian, Exponential, Landau or Polynomial. These PDFs can be easily joined together with intuitive interpretation of fraction coefficients, they allow construction of higher dimensional PDFs out of lower dimensional building block and describe correlations between observables. Again, many examples, documentation and downloadable binaries/source codes can be found on the RooFit website [21] or on the dedicated part of the ROOT website [22].

# Chapter 4

# Analysis overview

## 4.1 $B$-physics and ATLAS early data

The main $B$-physics analysis code is implemented as Athena tools and algorithms, and processes AOD/ESD files (see 3.5.1). The minimum requirement is that the code has access to *TrackParticles*, *Primary Vertices*, *Muons* and *Trigger* information. Analyses on Monte Carlo data will normally make use of *Truth* information as well.

A single Athena algorithm searches in the reconstructed AOD/ESD data for a given decay process (e.g. $B_s \to J/\psi(\mu\mu)\phi$). The output is in the form of ROOT n-tuples which contain a list of all possible candidates of the decay being sought, with full information on each part of the decay tree down to the tracks. Final analysis (including tuning cuts and all statistical analysis) should be performed on these ROOT n-tuples using ROOT scripts. The general technique is therefore to keep cuts in the Athena analysis as broad as possible [31].

$B$-physics analyses rely heavily on vertexing at the analysis stage, not just to calculate lifetimes of decay candidates, but also to reject incorrect combinations of tracks. However for the first stage of ATLAS datataking, for so-called *Early data*, $B$-physics analysis code makes composite particle candidate from any pair of decay products - in the case of $J/\psi$ candidate (i.e. di-muon), the algorithm takes all possible pairs of muons in the given event, independently of the vertices they come from. This could lead to meaningless combinations (in terms of invariant mass or momentum of composite particle) and thus to enhancement of the background. On the other hand this *flexibility* of the code seems to be more an advantage on the beginning since the code could not be tested on the real data before. Especially the question of primary vertices pile-up could not be answered on the Monte Carlo (MC) basis - therefore some supporting studies had to be done before actual testing (see 4.3).

## 4.2 Data selection

The ATLAS detector has been taking data since its completion in 2008. In the first phase the cosmic rays were measured and used for testing and calibrations. Then the first collisions came and ATLAS took real data at 900 GeV in 2009 and at the beginning of 2010. After that LHC has increased collision energy to 7 TeV. All 2010 7 TeV data from **STACO Muon** stream were used for presented studies. Lists of used data files are in appendix A. All of them are available on the Grid. Trigger settings were different in each period, summarized information are in Tab. 4.1.

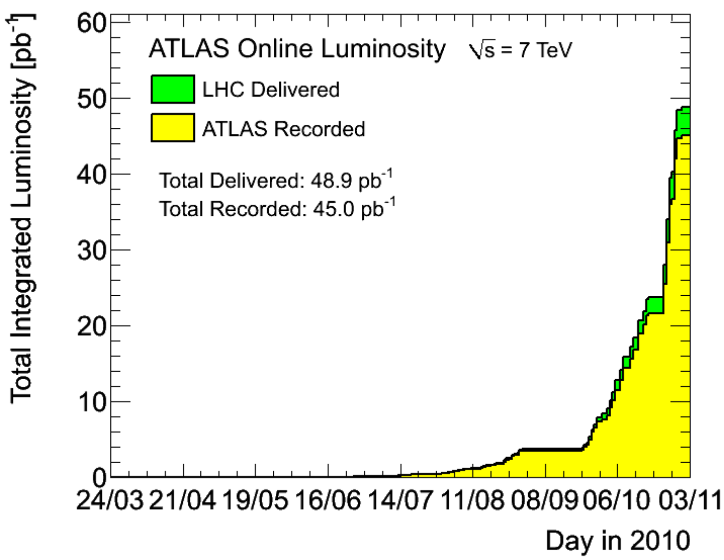


Figure 4.1: Integrated LHC/ATLAS luminosity taken through the year 2010. Figure from [33].

## 4.3 Primary vertices

On the ATLAS experiment the reconstruction of primary vertices is organized in two steps and made by two different algorithms: a) the primary vertex finding algorithm, dedicated to associate reconstructed tracks to the vertex candidates, and b) the vertex fitting algorithm, dedicated to reconstruct the vertex position and its corresponding error matrix. It also refits the associated tracks constraining them to originate from the reconstructed interaction point.

As shown on the Fig. 4.2, primary vertex resolution varies on the number of tracks used to build it. For 70 tracks the resolution is about 30 $\mu$m in transverse

| Period | Excluded runs | Trigger |
|---|---|---|
| B (153565 - 155160) | 153565 and 153599 | L1_MU0 |
| C (155228 - 156682) | - | L1_MU0 |
| D (158045 - 159224) | 158443 - 159113 | L1_MU0 |
| E (160387 - 161948) | 160387 - 161118 | EF_mu4 |
| F (162347 - 162882) | - | EF_mu6 |
| G (165591 - 166383) | - | EF_mu4_DiMu *or* |
| | | EF_mu4_Jpsimumu *or* |
| | | EF_mu4_Upsimumu_FS |
| H (166466 - 166964) | - | EF_2mu4_DiMu *or* |
| | | EF_2mu4_Jpsimumu *or* |
| | | EF_2mu4_Upsimumu |
| I (167575 - 167844) | - | EF_2mu4_DiMu *or* |
| | | EF_2mu4_Jpsimumu *or* |
| | | EF_2mu4_Upsimumu |

Table 4.1: Periods/runs used for analysis with trigger settings applied. Periods B to I contain all ATLAS 2010 7 TeV data.

plane and 50 $\mu$m in longitudinal direction, however for the minimal number of used tracks (3) it is about few milimeters [36].

After this general ATLAS vertex fitting, $B$-physics code refits the vertex again - once the di-muon candidate is created, its tracks are "taken out" from the original set of track used to built primary vertex and this vertex is then refitted again. Otherwise the distance between the primary vertex and the composite particle candidate vertex would be always zero.

The ATLAS reconstruction software distinguishes many types of primary vertices (there could be more than one primary vertex in given event), for this study only three of them are important:

- **primary vertex with status 1**: a vertex with the highest sum of $p_T^2$; only one vertex of this type per event
- **primary vertex with status 3**: a rest of vertices (but *NOT* secondary vertices); so-called *pile-up vertices*; zero or more per event
- **primary vertex with status 0**: "contains" tracks which were not used to built any other primary vertex; it has the parameters of the primary vertex

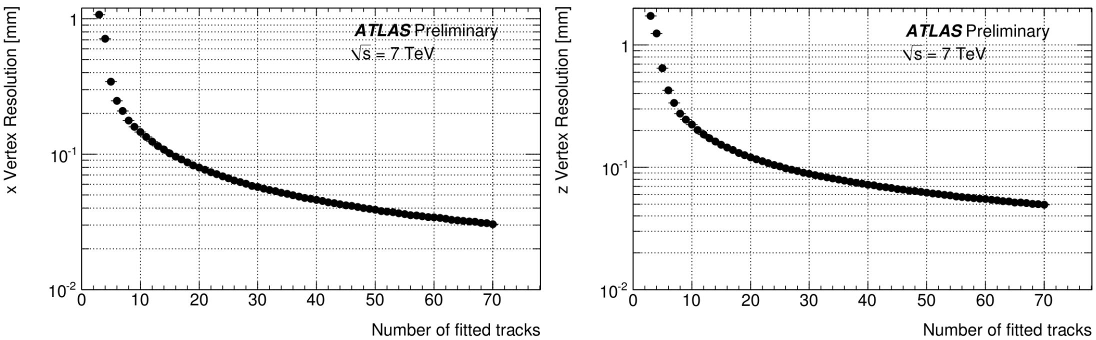


Figure 4.2: Estimated vertex resolutions $\sigma_{x_{PV}}$ (left) and $\sigma_{z_{PV}}$ (right) in 7 TeV data as a function of the number of tracks. Figures from [36].

with status 1 if it exists or the beamspot if not; so-called *dummy vertex*; one per event

## 4.4 $J/\psi$ candidate selection

Each possible "$J/\psi$ event" is required to contain at least one primary vertex built from at least three tracks, each of which containing at least one measurement in the Pixel detector and at least six in the SCT. In each surviving event, all pairs of oppositely-charged reconstructed muons are formed. From these two muons a "$J/\psi$ vertex" is built. To pass to the next step this vertex has to fulfil the cut $\chi^2/NDF < 10$.

From muons in given pair only these associated with ID tracks having at least one hit in the Pixel detector and six hits in the SCT are accepted. Also at least one combined muon is required to be in the pair. In terms of $p_T$ cuts, a harder muon has to have $p_T > 4.0$ GeV and a softer one $p_T > 2.5$ GeV.

As written above, a $J/\psi$ candidate can be made from *any* pair of muons. What more, these muons can come from different vertices in general. There are several possible combinations (i.e. combinations that could contain some "physics"):

- **PV(1)**: both muons come from primary vertex with status 1
- **PV(3)**: both muons come from primary vertex with status 3 (i.e. pile-up primary vertex)
- **PV(1)+PV(3)**: one muon comes from primary vertex with status 1 and the second one from primary vertex with status 3

- **PV(3)+PV(3')**: one muon comes from primary vertex with status 3 and the second one from some other primary vertex with status 3
- **PV(1)+unAs.**: one muon comes from primary vertex with status 1 and the second one is unassociated (i.e. its track was not used to built any primary vertex)
- **PV(3)+unAs.**: one muon comes from primary vertex with status 3 and the second one is unassociated
- **unAs.+unAs.**: both muons are unassociated

Some of them can be meaningless, but nobody could tell before real data were taken (for example, one primary vertex could be mistakenly divided in two by the vertex finding algorithm). Nobody has also tried to predict how the vertices pile-up would be and what would be its impact to measurements. To decide which combinations should be used it was the first task before actual $J/\psi$ measurements.

## 4.5 $J/\psi$ candidate mass fitting

Once the $J/\psi$ candidate is created and the vertex fit applied, the refitted track parameters and error matrices are used to calculate the invariant mass and its error. An unbinned maximum likelihood fit is then used to extract the mean reconstructed mass and the number of $J/\psi$ signal candidates from the data. The likelihood function $L$ is defined by

$$L = \prod_{i=1}^{N} [a_0 f_{J/\psi}(m^i_{\mu\mu}, \delta m^i_{\mu\mu}) + b_0 f_{\psi(2S)}(m^i_{\mu\mu}, \delta m^i_{\mu\mu}) + (1 - a_0 - b_0) f_{bkg}(m^i_{\mu\mu}, \delta m^i_{\mu\mu})] \tag{4.1}$$

where $N$ is the total number of oppositely charged muon pairs in the invariant mass range $2.5 < m_{\mu\mu} < 4.2$ GeV, $a_0$ and $b_0$ are fractions of pairs originating from $J/\psi$ and $\psi(2S)$ respectively and $f_{J/\psi}$, $f_{\psi(2S)}$ and $f_{bkg}$ are PDFs (see 3.5.3) that model $J/\psi$ , $\psi(2S)$ and background respectively. The $\psi(2S)$ resonance is fitted just because of better modelling of $J/\psi$ signal tails (since $\psi(2S)$ is very close to $J/\psi$ peak). For the signal, the mass is modelled with a Gaussian distribution

$$f_{sig}(m^i_{\mu\mu}, \delta m^i_{\mu\mu}) = \frac{1}{\sqrt{2\pi} S \delta m^i_{\mu\mu}} \mathrm{e}^{-\frac{(m^i_{\mu\mu} - m_{sig})^2}{2(S\delta m^i_{\mu\mu})^2}} \tag{4.2}$$

where $sig$ can be $J/\psi$ or $\psi(2S)$ and $S$ is a free parameter of the fit. For background, the 2$^{\text{nd}}$ order Chebychev polynomials have been used. The fit returns all necessary parameters: a mean di-muon mass $m_{\mu\mu}$, a fraction $a_0$ or $N_{sig}$ and $N_{bkg}$, scaling parameter $S$ and a covariance matrix of the fit. The mass resolution $\sigma_{m_{\mu\mu}}$ is then calculated as the half size of the interval $(m_{\mu\mu} \pm \sigma_{m_{\mu\mu}})$ for which the integral of the final curve retains 68.27 % of $N_{sig}$.

## 4.6 Autumn 2010 Reprocessing

The ATLAS data reprocessing campaign is an exercise in trying to resolve the tension between having stable reconstruction software for physics analysis and taking advantage of the constant improvements of the software algorithms, the calibration and alignment improvements and in the detector simulation. A full reprocessing campaign involves reconstructing all the raw ATLAS data with an updated software release.

Since before autumn 2010 reprocessing the Athena releases 15.6.9.8 and 15.6.9.9 were used for the RAW→ESD reconstruction, after that this switches to releases 16.0.2.3 and 16.0.2.5 (and partially release 16.0.2.7 for recover data from the latest crashed jobs). Detailed information about this reprocessing campaign can be found on dedicated website [34].

In the $B$-physics, reprocessing can have effect on reconstructed $J/\psi$ resonance width and also on the invariant mass shifts and its strange dependencies on various quantities such as $p_T$ (as presented in the chapter 6).

# Chapter 5

# Results of primary vertices study

As was written in the chapter 4, understanding of the primary vertices plays a crucial role in $B$-physics measurements. Summary of a supporting study of this topic is presented here - in terms of relations between various aspects of primary vertices and $J/\psi$ candidates in real LHC/ATLAS data.

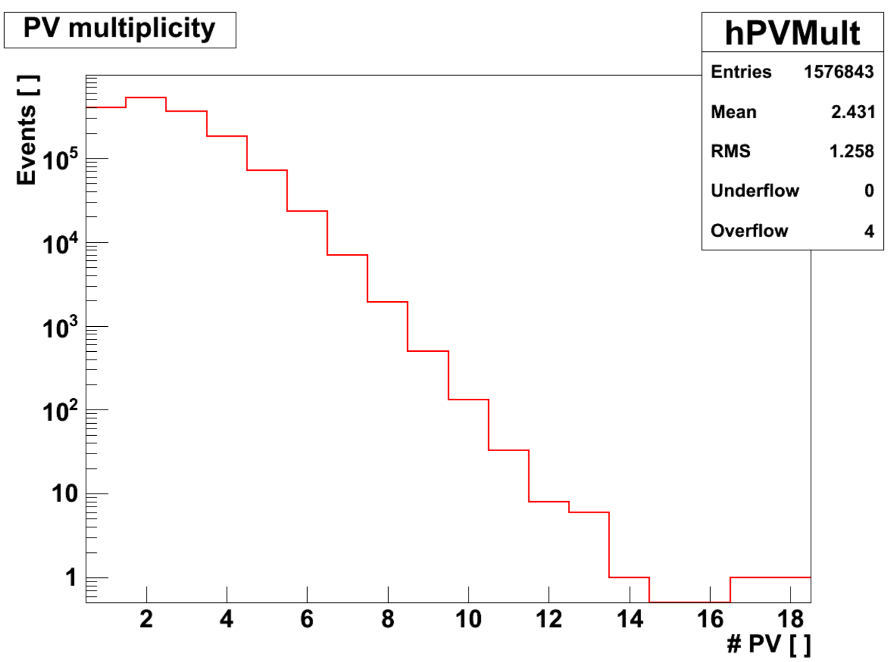


Figure 5.1: Primary vertex multiplicity, sum over all periods. Most of events have two primary vertices, but the number of events with more than 10 is also significant. Primary vertex multiplicity for each period separately can be found in appendix B, Figs. B.1 and B.2.

At the beginning of LHC/ATLAS 7 TeV phase, the problem of multiple primary vertices was not so important since there was very low luminosity. As you can see in the appendix B in Fig. B.1, in the period B of ATLAS runs there were only few events with more than two primary vertices. However with increasing luminosity the problem became more significant (see Figs. B.1 and B.2 in the appendix B). Sum of all 2010 periods is shown in Fig. 5.1 - as you can see the multiplicity is very high. With this number of primary vertices in one event, the possibility of a wrong association of tracks to vertices grows up rapidly. Also a possibility of strange combinations of muon pairs (i.e. muons coming from two different vertices, see 4.4) become significant, as you can see in Fig. 5.2 (sum ovew all 2010 periods) or in Figs. B.3 and B.4 in the appendix B (each period separately). However some of these "strange combinations" (all except **same PV(1)** and **same PV(3)**) actually *can* contain some "physics information", i.e. real $J/\psi$ candidates.

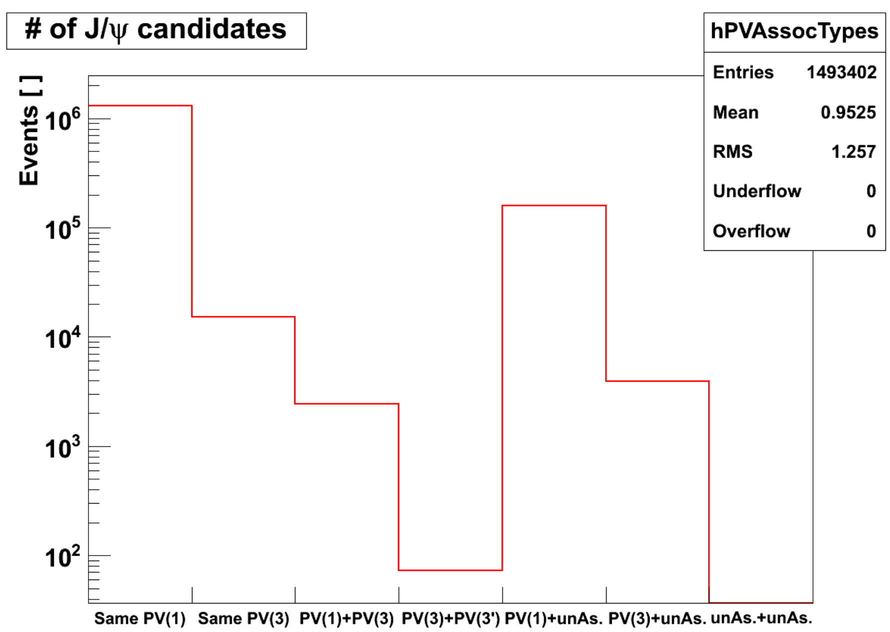


Figure 5.2: Number of $J/\psi$ candidates (di-muons) for various primary vertices combinations (see 4.4), sum over all periods. Unfortunately the number of "strange combinations" (all except **same PV(1)** and **same PV(3)**) considerable. Same plots for each period separately can be found in appendix B, Figs. B.3 and B.4.

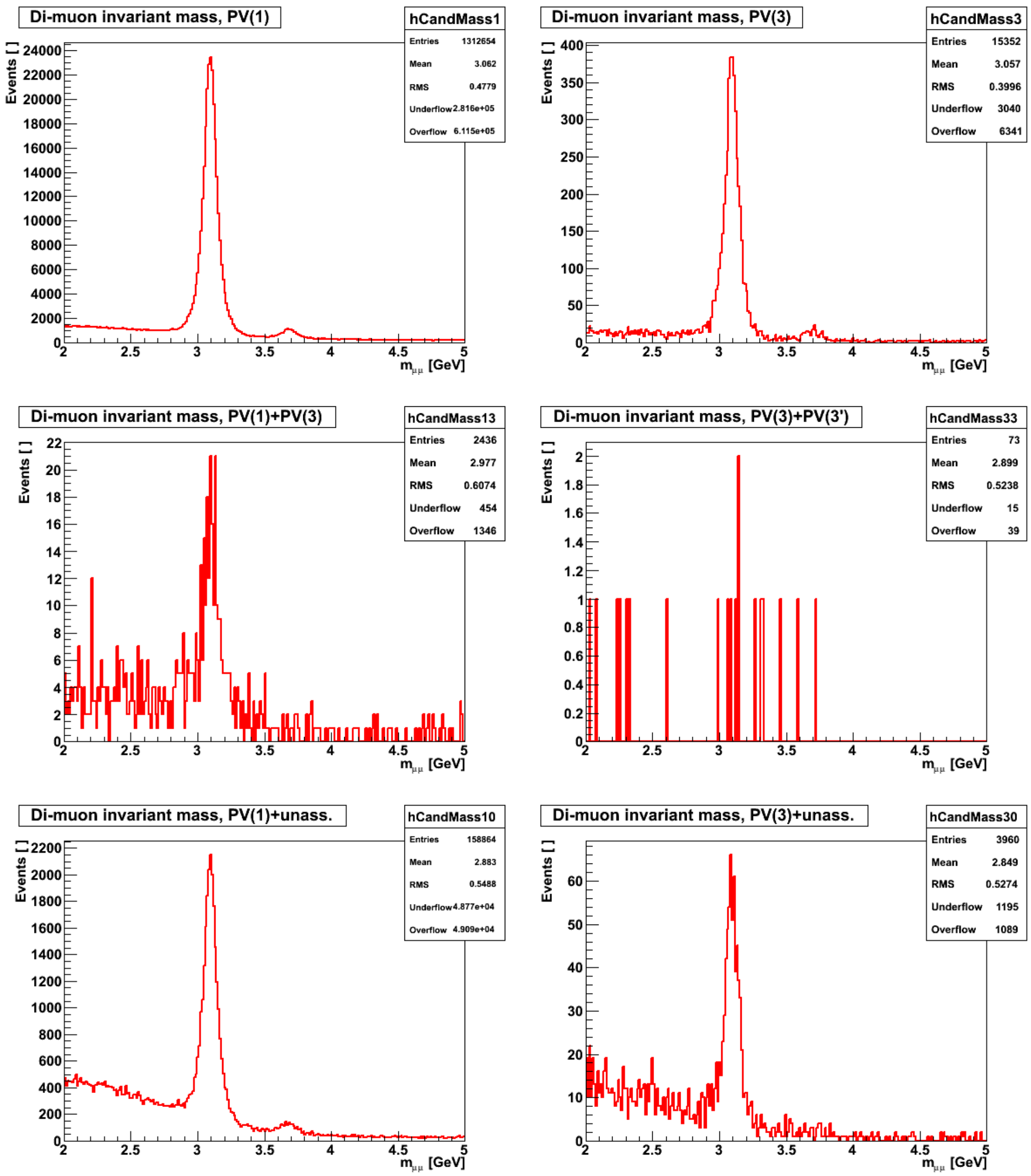


Figure 5.3: Di-muon invariant mass for various primary vertices combinations (see 4.4). **PV(1)+PV(3)** and **PV(3)+PV(3')** combinations (the second row) contain very low number of real $J/\psi$ candidates and thus could be expelled from further analysis. What is surprising is that the invariant mass spectrum of candidates with one track unassociated (the bottom row) contain very nice $J/\psi$ peaks and thus could be counted in.

Di-muon invariant mass spectra for each possible primary vertices combination are shown in Fig. 5.3. **PV(1)+PV(3)** and **PV(3)+PV(3')** combinations contain very low number of real $J/\psi$ candidates and thus could be expelled from further analysis. What is surprising is that the invariant mass spectrum of candidates with one track unassociated contain very nice $J/\psi$ peaks and thus could be counted in. To find the probable reason of this unassociation of one track, one should look onto track parameters (see 3.1) of these muons (Fig. 5.4). Very large $d_0$ impact parameter could be caused by non-promt $J/\psi$ (it could decay at a larger distance from the interaction point and thus the muon track does not point to any primary vertex).

Just to show that **PV(1)+PV(3)** and **PV(3)+PV(3')** combinations really do not contain much usable signal and thus can (and should) be excluded from the next analysis, distances and their errors between primary vertices in these events are shown in Fig. 5.5. As one can see, $z$ distances between vertices are so large that it cannot be only the vertex algorithm misassignment.

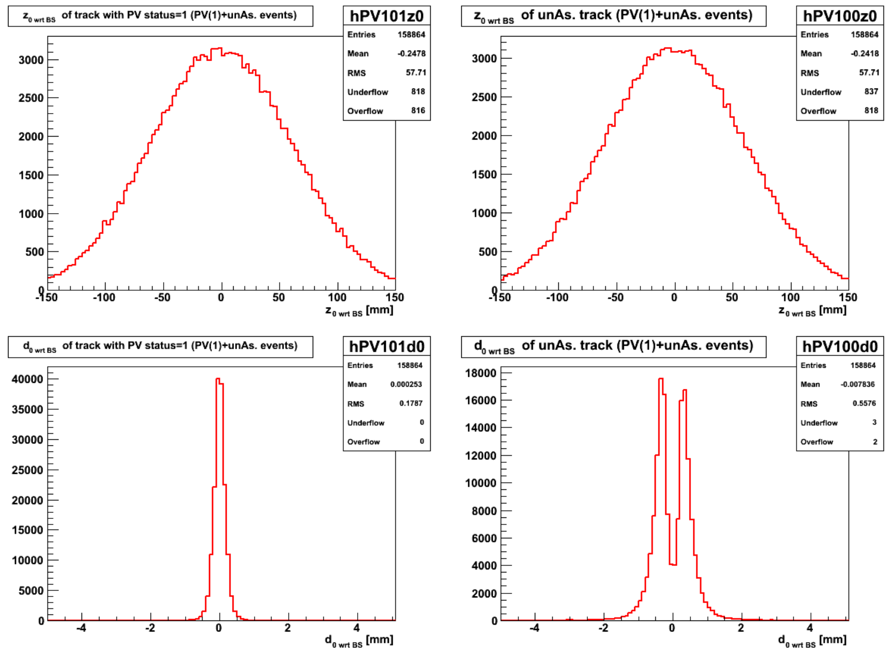


(a)

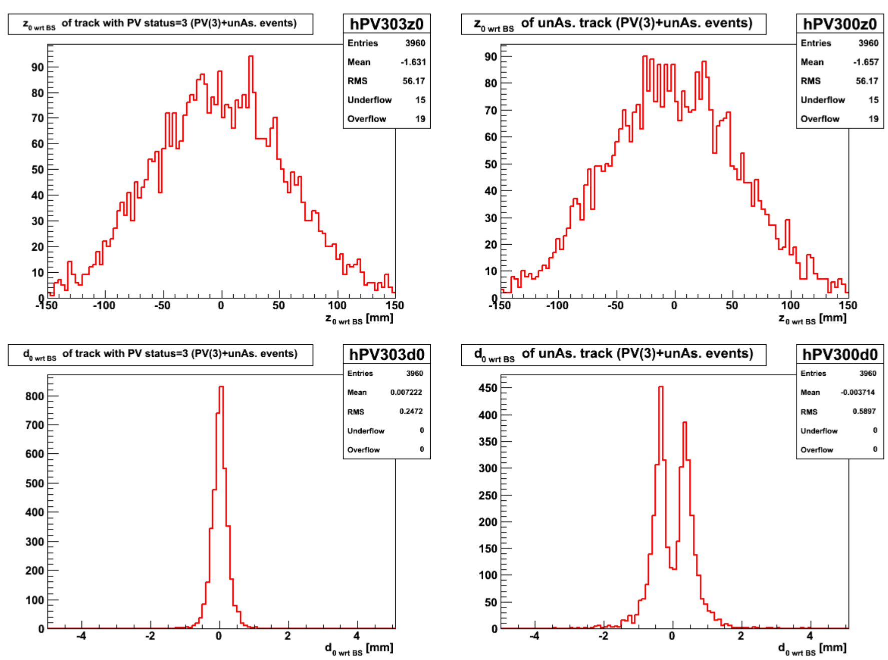


(b)

Figure 5.4: Track parameters (see 3.1) - with respect to the beam spot - of muons from **PV(1)+unAs.** (a) and **PV(3)+unAs.** (b) candidates. The reason why these tracks are unassociated is probably very large $d_0$ impact parameter - $J/\psi$ candidate could decay at a larger distance from the interaction point and thus the muon track does not point to any primary vertex.

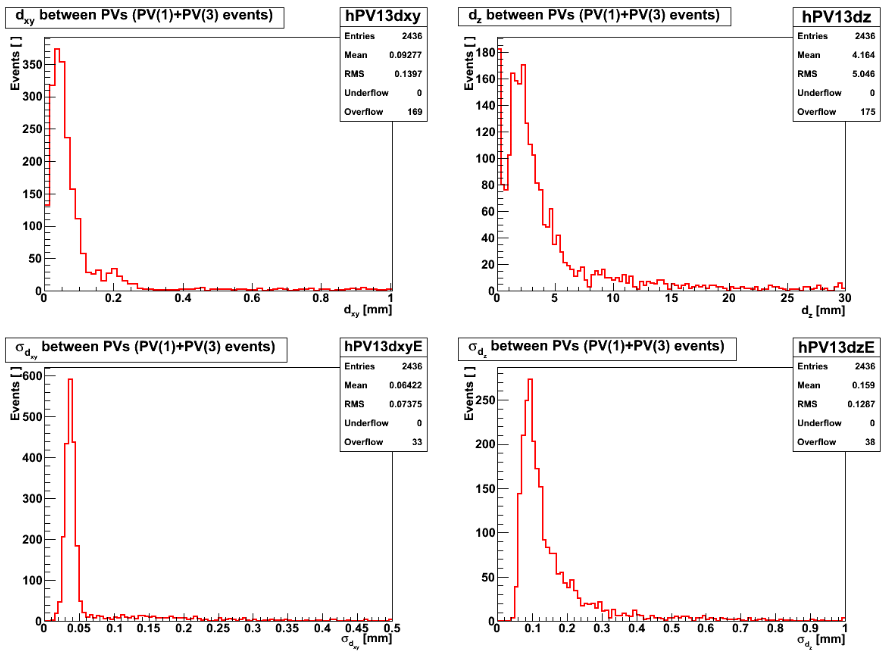


(a)

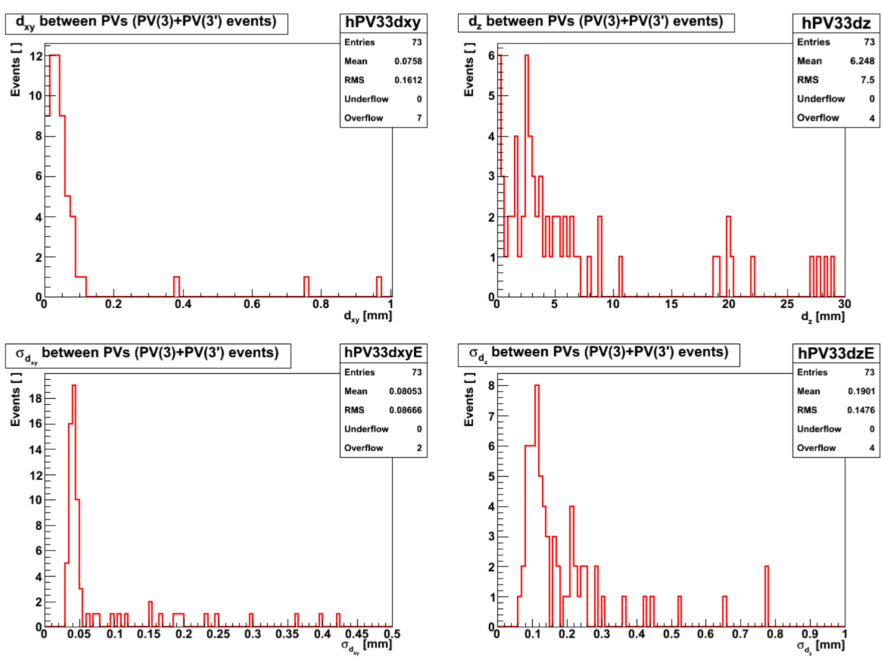


(b)

Figure 5.5: Distances and their errors between primary vertices in **PV(1)+PV(3)** (a) and **PV(3)+PV(3')** (b) events. As one can see, $z$ distances between vertices are so large that it cannot be only the vertex algorithm misassignment.

# Chapter 6

# $J/\psi$ events in Inner Detector performance

According to results presented in the chapter 5, **PV(1)+PV(3)** and **PV(3)+PV(3')** combinations have been excluded from the following analysis. It is focused on $J/\psi$ peak and its width and position in the invariant mass spectrum. $J/\psi$ PDG mass is $(3096.916 \pm 0.011)$ MeV and $\psi(2S)$ mass is $(3686.09 \pm 0.04)$ MeV [1].

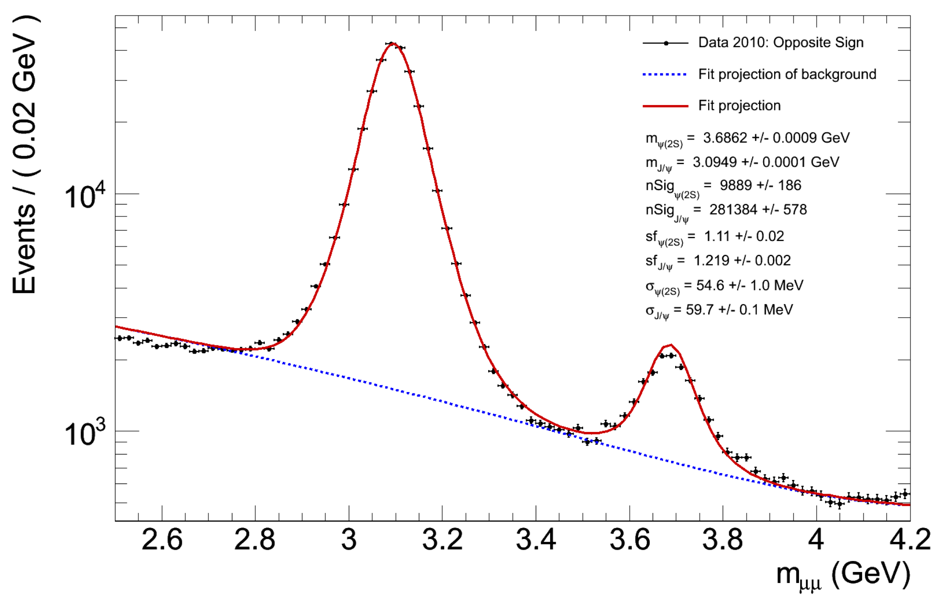


Figure 6.1: Fit of the di-muon invariant mass distribution, all 2010 7 TeV data.

Fig. 6.1 shows very precise fit (note the log scale) of di-muon invariant mass spectrum. As you can see, both peaks ($J/\psi$ and $\psi(2S)$) have very good shape and width, but the position of $J/\psi$ peak is shifted left (i.e. to lower mass) about 2 MeV (about 0.07 %). What is strange is that the $\psi(2S)$ peak is at the right position. It means that not the whole di-muon spectrum, but only the $J/\psi$ peak is shifted. On the other hand, the fit of $\psi(2S)$ is not so perfect.

There is no explanation why only the $J/\psi$ part of the spectrum is shifted and thus I think we can presume that the precision of the $\psi(2S)$ fit is low and that the whole spectrum is shifted. In this case, one possible reason could be using wrong muon mass in a calculation of di-muon invariant mass, for example because of some error during reading the PDG database. I have tested this possibility, but the whole process of the invariant mass calculation is correct. Thus only the possibility of wrongly measured/calculated muons quantities (e.g. $p_T$ of muons) remains. In next sections we will have closer look onto the possible dependencies of $J/\psi$ invariant mass on the detector.

## 6.1 $J/\psi$ candidate invariant mass in different detector regions

The ATLAS detector could be divided according to $\eta$ of a particle into so-called *barrel* ($\eta \leq 1.05$) and *end-cap* ($\eta > 1.05$) regions. Following figures show the $J/\psi$ mass fits for three combination of muons: both muons are in the barrel region (Fig. 6.2), one muon is in the barrel region and the other is in the end-cap (Fig. 6.3) and both muons are in the end-cap region (Fig. 6.4). As you can see, the peak position is shifting left and becoming wider just in this order. We can thus say that the barrel region of the ATLAS detector is more precise than the end-cap regions (from where most of events unfortunately come). However this is expected due to the detector geometry.

## 6.2 $J/\psi$ candidate invariant mass - $p_T$, $\eta$ and $\phi$ binning

Invariant mass as a function of various $J/\psi$ candidate kinematic quantities can also give us very important informations about the detector performance.

As you can see in Fig. 6.5 there are no detectable $J/\psi$ candidates with $p_T < 5$ GeV. And those with the lowest possible $p_T$ have a very bad reconstructed mass and resolution (peak width) too. Situation becomes better around 10 GeV. Whilst the mass dependency on the $\phi$ coordinate is relatively uniform (see Fig. 6.7), not so the dependency on $\eta$ (Fig. 6.6). Unexpectable dip can be seen around $\eta = 1.6$. Since the resolution is absolutely normal in this bin, the reason cannot be any hardware problem. The dip is probably caused by the wrong detector (material) description, i.e. software problem. Similar studies have been made also by other groups with

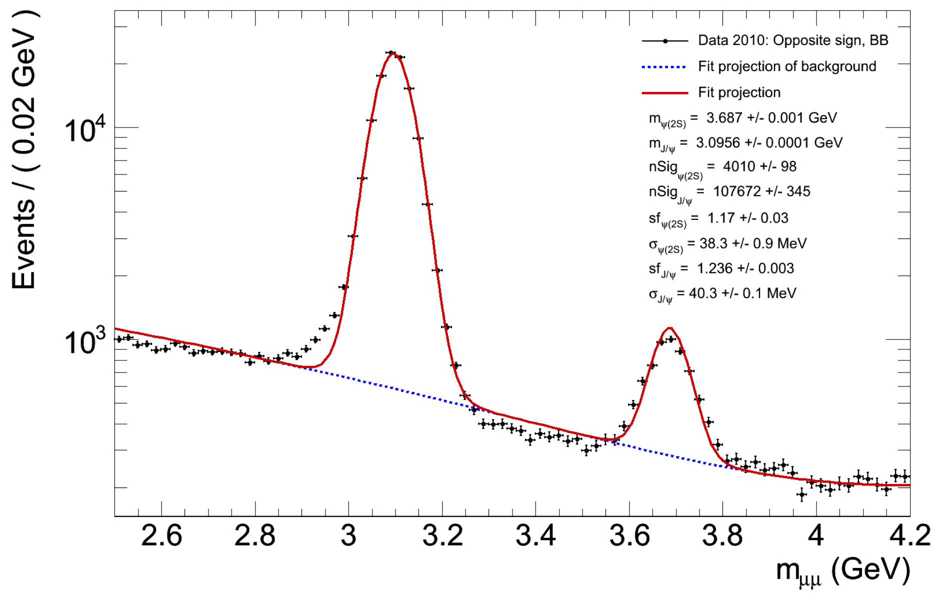


Figure 6.2: Fit of the di-muon invariant mass distribution, both muons in the barrel region.

the same results and thus the detector group is hardly working on the solution, but as we will see in the last section of this chapter, for the time being with no success.

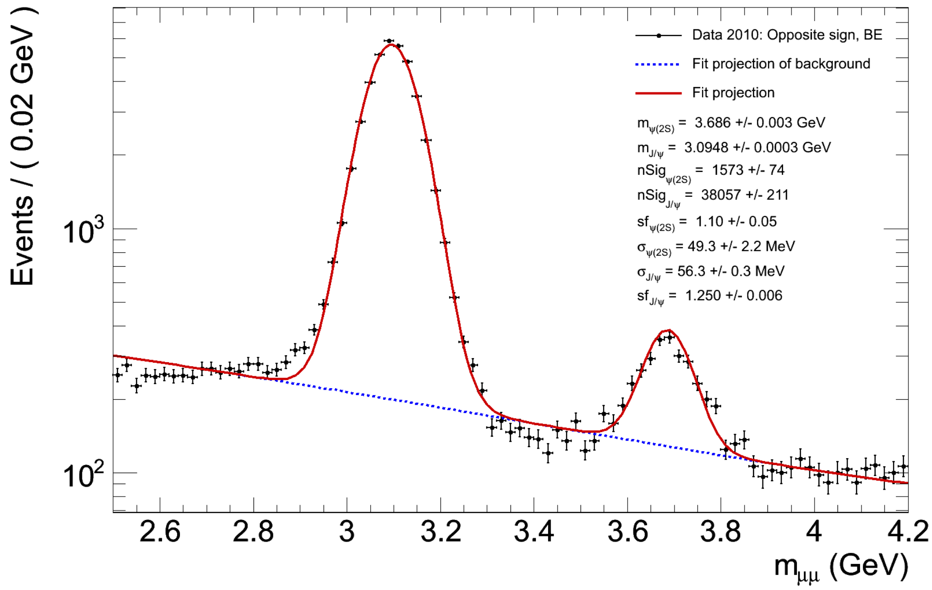


Figure 6.3: Fit of the di-muon invariant mass distribution, one muon in the barrel region, the other in the end-cap region.

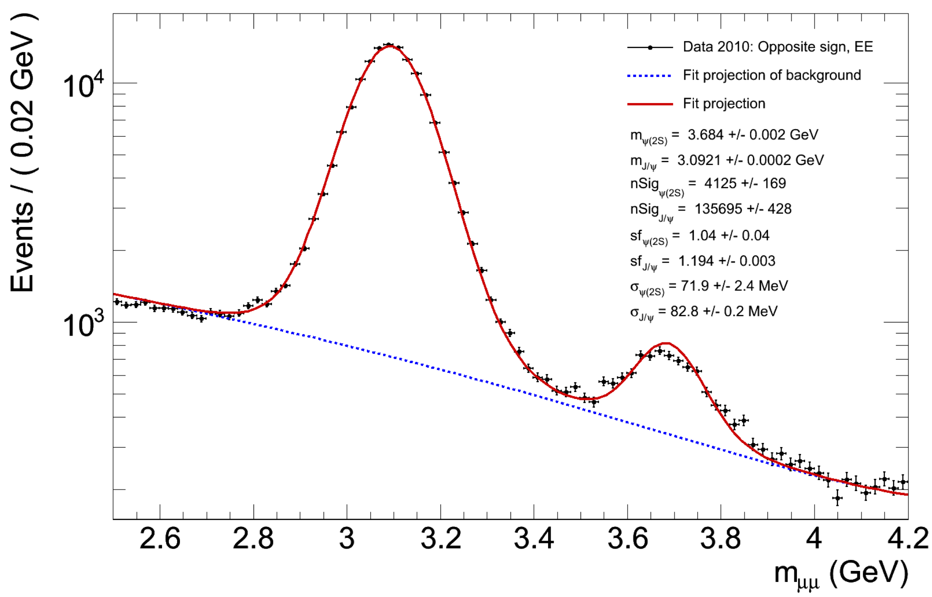


Figure 6.4: Fit of the di-muon invariant mass distribution, both muons in the end-cap regions.

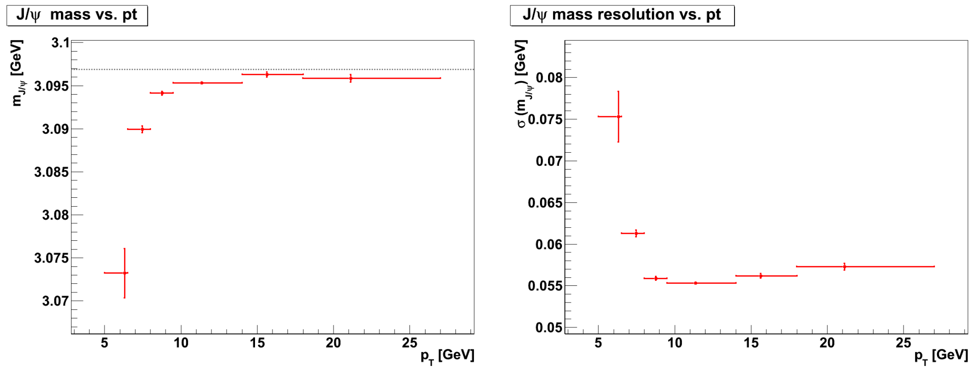


Figure 6.5: Results of $J/\psi$ candidate mass fit as a function of $J/\psi$ candidate $p_T$.

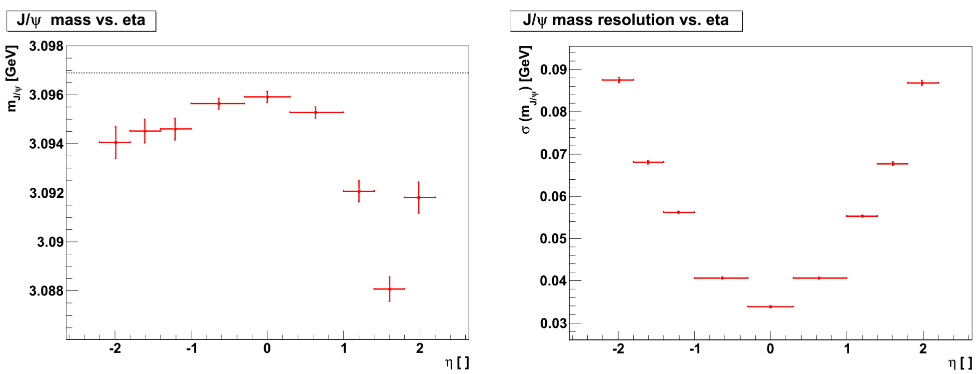


Figure 6.6: Results of $J/\psi$ candidate mass fit as a function of $J/\psi$ candidate $\eta$.

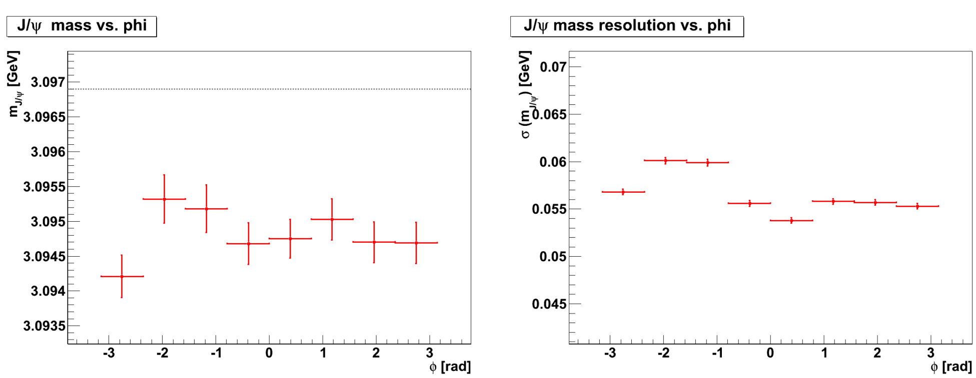


Figure 6.7: Results of $J/\psi$ candidate mass fit as a function of $J/\psi$ candidate $\phi$.

## 6.3 Comparison of the detector performance before and after Autumn 2010 Reprocessing

The same study as presented in the first two section of this chapter has been made also for reprocessed data (see section 4.6). As you can see in the following plots, the Autumn 2010 reprocessing has unfortunately not the expected effect to the $J/\psi$ peak position problem. In reprocessed data the whole invariant mass spectrum is shifted about 2 MeV left from the previous state (i.e. now the $J/\psi$ peak is shifted about 4 MeV and the $\psi(2S)$ peak about 2 MeV). However this new shift is not uniform in terms of the shifting the whole $p_T/\eta/\phi$ dependency (see Figs. 6.12, 6.12 and 6.14). On the other hand, $J/\psi$ peak resolution has improved, in other words after reprocessing we have precisely measured wrong values. Summary of this comparison is in Tab. 6.1.

| | | Before repro. | After repro. | PDG mass [MeV] |
|---|---|---|---|---|
| All data | $m_{J/\psi}$ [MeV] | $3094.9 \pm 0.1$ | $3093.4 \pm 0.1$ | $3096.916 \pm 0.011$ |
| | $\sigma_{m_{J/\psi}}$ [MeV] | $59.7 \pm 0.1$ | $58.1 \pm 0.1$ | |
| BB reg. | $m_{J/\psi}$ [MeV] | $3095.6 \pm 0.1$ | $3093.8 \pm 0.1$ | |
| | $\sigma_{m_{J/\psi}}$ [MeV] | $40.3 \pm 0.1$ | $39.0 \pm 0.1$ | |
| BE reg. | $m_{J/\psi}$ [MeV] | $3094.8 \pm 0.3$ | $3093.4 \pm 0.3$ | |
| | $\sigma_{m_{J/\psi}}$ [MeV] | $56.3 \pm 0.3$ | $54.3 \pm 0.3$ | |
| EE reg. | $m_{J/\psi}$ [MeV] | $3092.1 \pm 0.2$ | $3092.0 \pm 0.2$ | |
| | $\sigma_{m_{J/\psi}}$ [MeV] | $82.8 \pm 0.2$ | $80.9 \pm 0.2$ | |

Table 6.1: Summary of comparisons between mass fits before and after reprocessing. PDG value taken from [1].

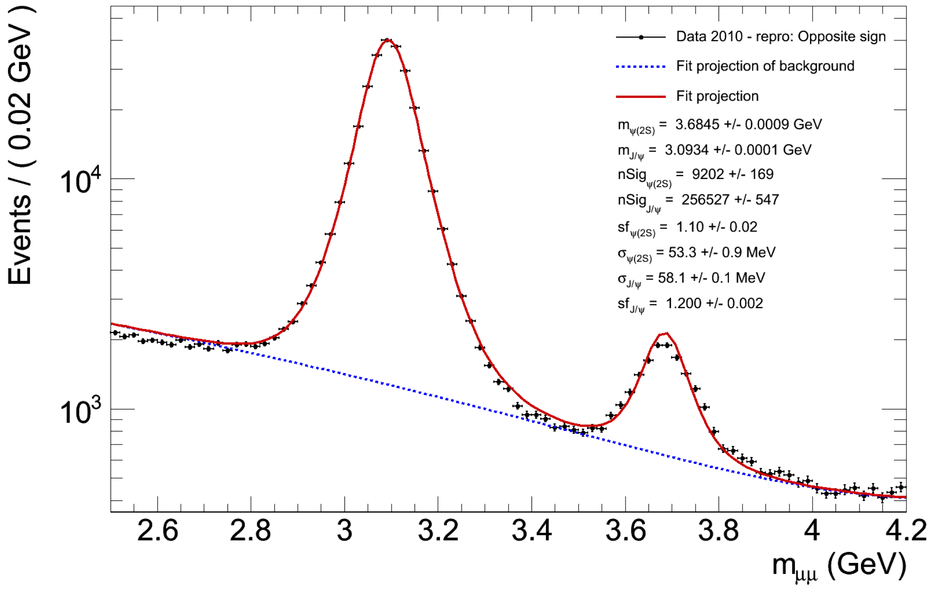


Figure 6.8: Fit of the di-muon invariant mass distribution, all 2010 7 TeV data after reprocessing. Fit results before reprocessing: $m_{J/\psi} = 3.0949$ GeV and $m_{\psi(2S)} = 3.6862$ GeV.

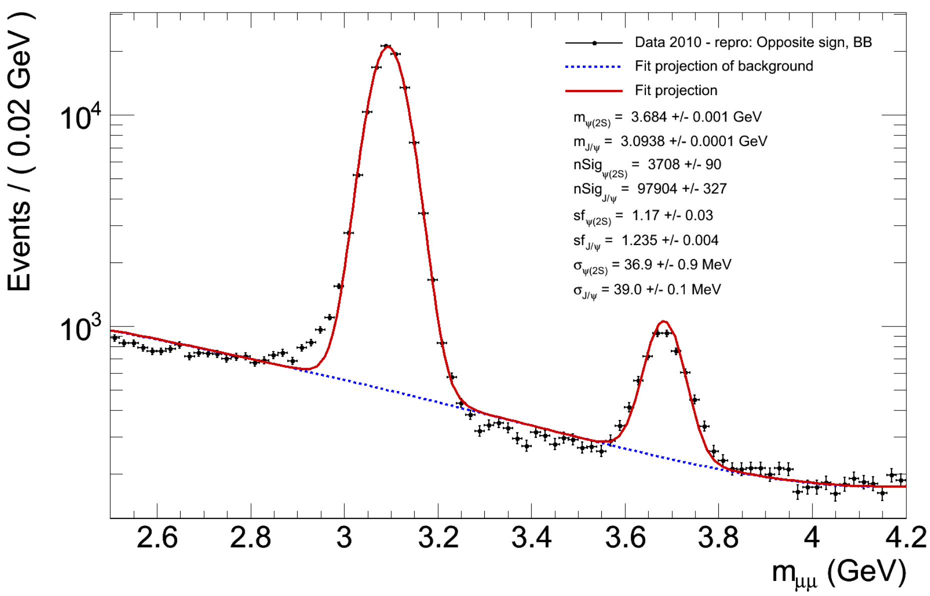


Figure 6.9: Fit of the di-muon invariant mass distribution, both muons in the barrel region, after reprocessing. Fit results before reprocessing: $m_{J/\psi} = 3.0949$ GeV and $m_{\psi(2S)} = 3.6862$ GeV.

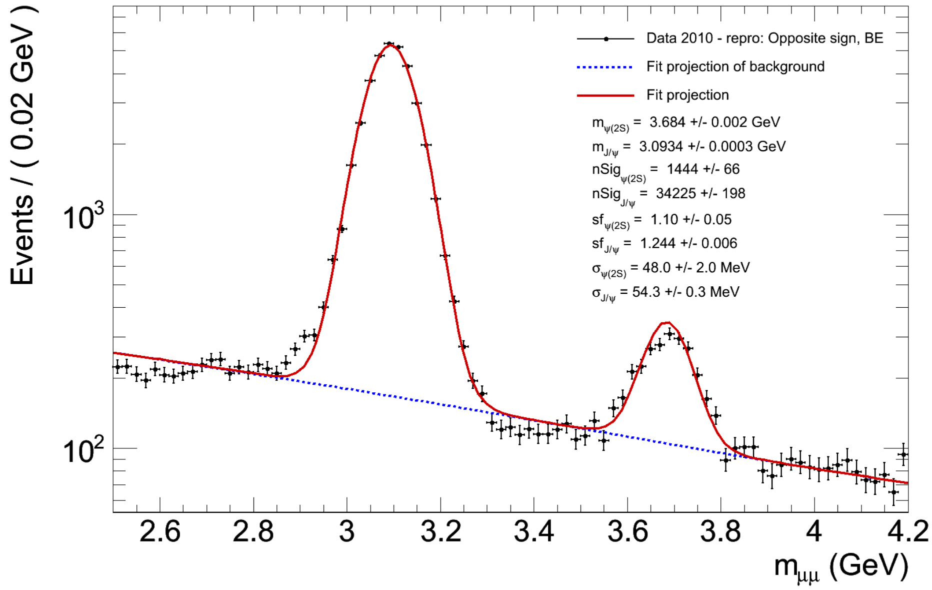


Figure 6.10: Fit of the di-muon invariant mass distribution, one muon in the barrel region, the other in the end-cap region, after reprocessing. Fit results before reprocessing: $m_{J/\psi} = 3.0956$ GeV and $m_{\psi(2S)} = 3.687$ GeV.

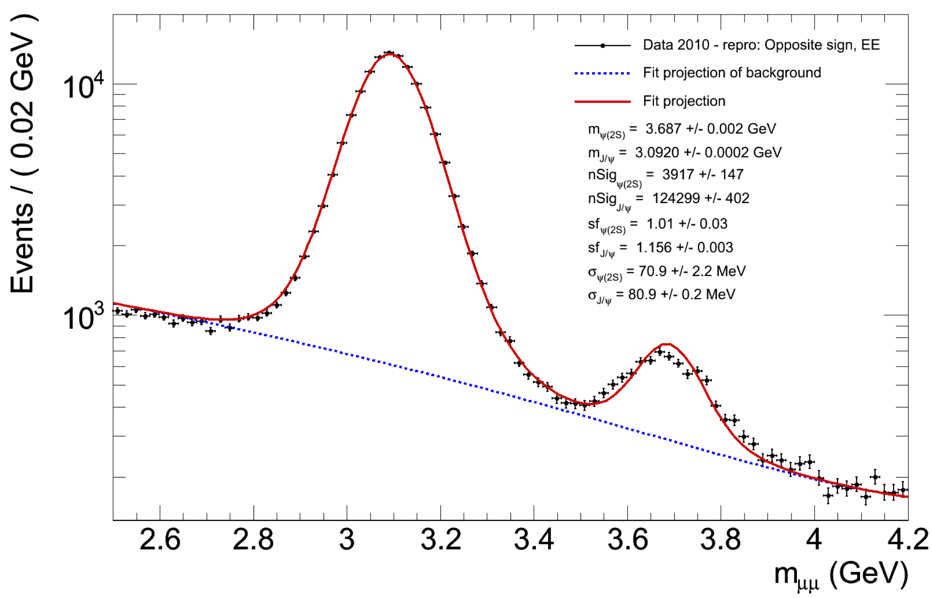


Figure 6.11: Fit of the di-muon invariant mass distribution, both muons in the end-cap regions, after reprocessing. Fit results before reprocessing: $m_{J/\psi} = 3.0948$ GeV and $m_{\psi(2S)} = 3.686$ GeV.

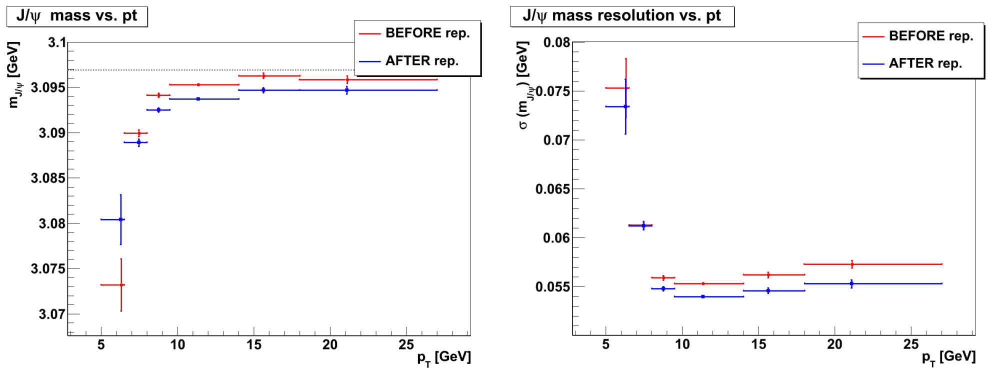


Figure 6.12: Comparison between $J/\psi$ candidate mass fit as a function of $J/\psi$ candidate $p_T$ before and after reprocessing.

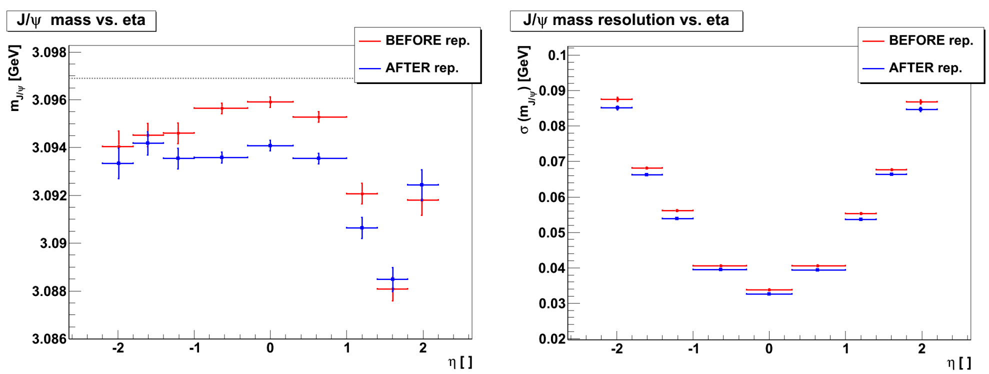


Figure 6.13: Comparison between $J/\psi$ candidate mass fit as a function of $J/\psi$ candidate $\eta$ before and after reprocessing.

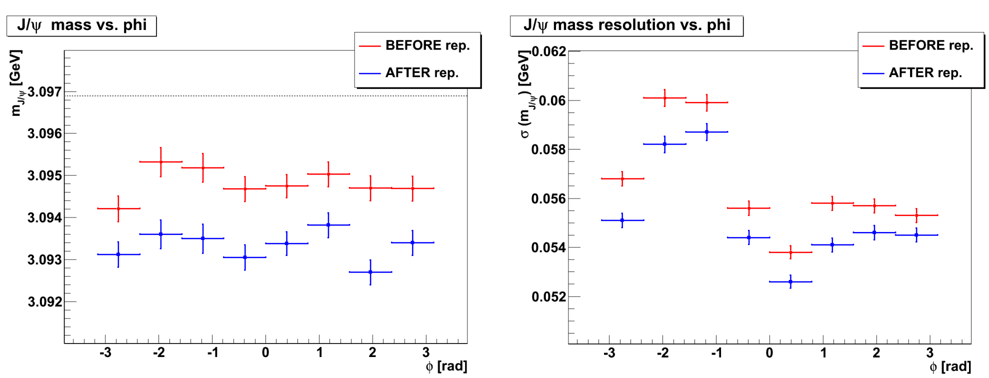


Figure 6.14: Comparison between $J/\psi$ candidate mass fit as a function of $J/\psi$ candidate $\phi$ before and after reprocessing.

# Chapter 7

# Conclusions

This thesis was devoted to testing the ATLAS detector performance using the $J/\psi$ resonance. For this purpose all ATLAS 2010 7 TeV data from proton-proton collisions were used (about 45 $\mathrm{pb}^{-1}$). Before the actual analysis it was necessary to do some supporting primary vertices studies, since the effects of multiple vertices to $J/\psi$ invariant mass were unknown as well as the effect of various muon pairs combinations with respect to the vertices they come from.

As shown in the chapter 5, only these $\mu^+\mu^-$ combinations should be used for physics analysis: a) both muon tracks are associated to the same primary vertex (does not matter if type 1 or 3, i.e. pile-up) or b) one muon track from the di-muon candidate could be unassociated (i.e. not pointing to any primary vertex). The rest of possible combinations do not contain any $J/\psi$ information or a yield is very poor.

The main part of the analysis is based on my work for the ATLAS $B$-physics group. In the chapter 6 the most important results were presented. Di-muon invariant mass spectrum shows very nice $J/\psi$ peak, but shifted about 2 MeV left to 3094.9 MeV. One can say that a relative error about 0.07 % is very good result. However with respect to the fit precision (see Fig. 6.1) and the peak width (59.7 MeV), I and neither the collaboration cannot agree with this statement. Another challenge is a dip in the dependency of $J/\psi$ mass on the $\eta$ coordinate (see Fig. 6.6). After a deeper look we can say that this dip and also the shift of $J/\psi$ mass peak position are both caused by some trigger or software rather than hardware effect. In the case of the $\eta$ dip it could also be a wrong detector description in the database for example. Both problems are still under investigation.

Autumn 2010 reprocessing of all ATLAS data should bring us improved results, but not all these expectations have been fulfilled. It is true that the $J/\psi$ mass peak resolution has improved, but on the other hand the whole di-muon invariant mass spectrum is shifted about another 2 MeV (about 4 MeV in total). Precise comparison between mass fits before and after reprocessing is presented in the last section of the chapter 6. All results are then summarised in Tab. 6.1.

However we can say that all these preliminary results of the ATLAS experiment are very good since it is the biggest and probably the most complicated particle detector ever built and is still on the beginning of its “journey”.

All results of this analysis were presented at several ATLAS meetings held at CERN ([25], [26], [27] and [29]) and also used by $B$-physics group for further studies and measurements (e.g. [30]). Another presentation of this work was performed at technical seminar at the Institute of Physics at the Academy of Sciences of the Czech Republic [28].

# Appendix A

# List of data files

## A.1 Before reprocessing

user.JamesCatmore.167844.f299_m644.Muons.v03-pass1-lhcstable.staco.EarlyOnia_EXT0/

user.JamesCatmore.167776.f299_m639.Muons.v03-pass1-lhcstable.staco.EarlyOnia_EXT0/

user.JamesCatmore.167680.f299_m639.Muons.v03-pass1-lhcstable.staco.EarlyOnia_EXT0/

user.JamesCatmore.167661.f299_m639.Muons.v03-pass1-lhcstable.staco.EarlyOnia_EXT0/

user.JamesCatmore.167607.f298_m639.Muons.v03-pass1-lhcstable.staco.EarlyOnia_EXT0/

user.JamesCatmore.167576.f298_m639.Muons.v03-pass1-lhcstable.staco.EarlyOnia.1_EXT0/

user.JamesCatmore.167575.f298_m634.Muons.v03-pass1-lhcstable.staco.EarlyOnia_EXT0/

user.JamesCatmore.166964.f296_m624.Muons.v03-pass1-lhcstable.staco.EarlyOnia.1_EXT0/

user.JamesCatmore.166927.f296_m624.Muons.v03-pass1-lhcstable.staco.EarlyOnia.1_EXT0/

user.JamesCatmore.166925.f296_m624.Muons.v03-pass1-lhcstable.staco.EarlyOnia_EXT0/

user.JamesCatmore.166924.f296_m624.Muons.v03-pass1-lhcstable.staco.EarlyOnia.1_EXT0/

user.JamesCatmore.166856.f296_m624.Muons.v03-pass1-lhcstable.staco.EarlyOnia_EXT0/

user.JamesCatmore.166850.f296_m624.Muons.v03-pass1-lhcstable.staco.EarlyOnia_EXT0/

user.JamesCatmore.166786.f296_m624.Muons.v03-pass1-lhcstable.staco.EarlyOnia_EXT0/

user.JamesCatmore.166658.f295_m624.Muons.v03-pass1-lhcstable.staco.EarlyOnia_EXT0/

user.JamesCatmore.166466.f295_m619.Muons.v03-pass1-lhcstable.staco.EarlyOnia_EXT0/

user.JamesCatmore.166383.f295_m619.Muons.v03-pass1-lhcstable.staco.EarlyOnia_EXT0/

user.JamesCatmore.166305.f295_m619.Muons.v03-pass1-lhcstable.staco.EarlyOnia_EXT0/

user.JamesCatmore.166198.f295_m619.Muons.v03-pass1-lhcstable.staco.EarlyOnia_EXT0/

user.JamesCatmore.166143.f294_m619.Muons.v03-pass1-lhcstable.staco.EarlyOnia_EXT0/

user.JamesCatmore.166142.f294_m619.Muons.v03-pass1-lhcstable.staco.EarlyOnia_EXT0/

user.JamesCatmore.166097.f294_m614.Muons.v03-pass1-lhcstable.staco.EarlyOnia_EXT0/

user.JamesCatmore.166094.f294_m614.Muons.v03-pass1-lhcstable.staco.EarlyOnia_EXT0/

user.JamesCatmore.165956.f294_m614.Muons.v03-pass1-lhcstable.staco.EarlyOnia_EXT0/

user.JamesCatmore.165954.f294_m614.Muons.v03-pass1-lhcstable.staco.EarlyOnia_EXT0/

user.JamesCatmore.165821.f293_m609.Muons.v03-pass1-lhcstable.staco.EarlyOnia_EXT0/

user.JamesCatmore.165818.f293_m609.Muons.v03-pass1-lhcstable.staco.EarlyOnia_EXT0/

user.JamesCatmore.165817.f293_m609.Muons.v03-pass1-lhcstable.staco.EarlyOnia_EXT0/

user.JamesCatmore.165815.f293_m609.Muons.v03-pass1-lhcstable.staco.EarlyOnia_EXT0/

user.JamesCatmore.165767.f293_m614.Muons.v03-pass1-lhcstable.staco.EarlyOnia_EXT0/

user.JamesCatmore.165732.f293_m609.Muons.v03-pass1-lhcstable.staco.EarlyOnia_EXT0/

user.JamesCatmore.165703.f293_m609.Muons.v03-pass1-lhcstable.staco.EarlyOnia.1_EXT0/

user.JamesCatmore.165632.f293_m609.Muons.v03-pass1-lhcstable.staco.EarlyOnia_EXT0/

user.JamesCatmore.165591.f292_m609.Muons.v03-pass1-lhcstable.staco.EarlyOnia_EXT0/

user.JamesCatmore.periodF.t0pro04_v01.Muons.v03-pass1-2010F_muon.staco.EarlyOnia.30_EXT0

user.JamesCatmore.periodE7.t0pro04_v01.Muons.v03-pass1-2010E_muon.staco.EarlyOnia.20_EXT0

user.JamesCatmore.periodE6.t0pro04_v01.Muons.v03-pass1-2010E_muon.staco.EarlyOnia.40_EXT0/

user.JamesCatmore.161379.f282_m578.Muons.v03-pass1-2010E_muon.staco.EarlyOnia.60_EXT0/

user.JamesCatmore.periodD1.t0pro04_v01.Muons.v03-pass1-2010D_RPCloose_muon.staco.EarlyOnia.20_EXT0

user.JamesCatmore.periodC.t0pro04_v01.Muons.v03-pass1-2010C_muon.staco.EarlyOnia.20_EXT0

user.JamesCatmore.periodB.repro04_v01.Muons.v03-repro04-01_muon.staco.EarlyOnia.20_EXT0

## A.2 After reprocessing

user.JamesCatmore.periodI.repro05_v02.Muons.v03-repro05-01.staco.EarlyOnia.3_EXT0/

user.JamesCatmore.periodH.repro05_v02.Muons.v03-repro05-01.staco.EarlyOnia.3_EXT0/

user.JamesCatmore.periodG.repro05_v02.Muons.v03-repro05-01.staco.EarlyOnia.3_EXT0/

user.JamesCatmore.periodF.repro05_v02.Muons.v03-repro05-01.staco.EarlyOnia.1_EXT0/

user.JamesCatmore.periodE.repro05_v02.Muons.v03-repro05-01.staco.EarlyOnia.3_EXT0/

user.JamesCatmore.periodD.repro05_v02.MuonswBeam.v03-repro05-01.staco.EarlyOnia.1_EXT0/

user.JamesCatmore.periodC.repro05_v02.MuonswBeam.v03-repro05-01.staco.EarlyOnia.3_EXT0/

user.JamesCatmore.periodB.repro05_v02.MuonswBeam.v03-repro05-01.staco.EarlyOnia.1_EXT0/

# Appendix B

# Study of primary vertices - per period plots

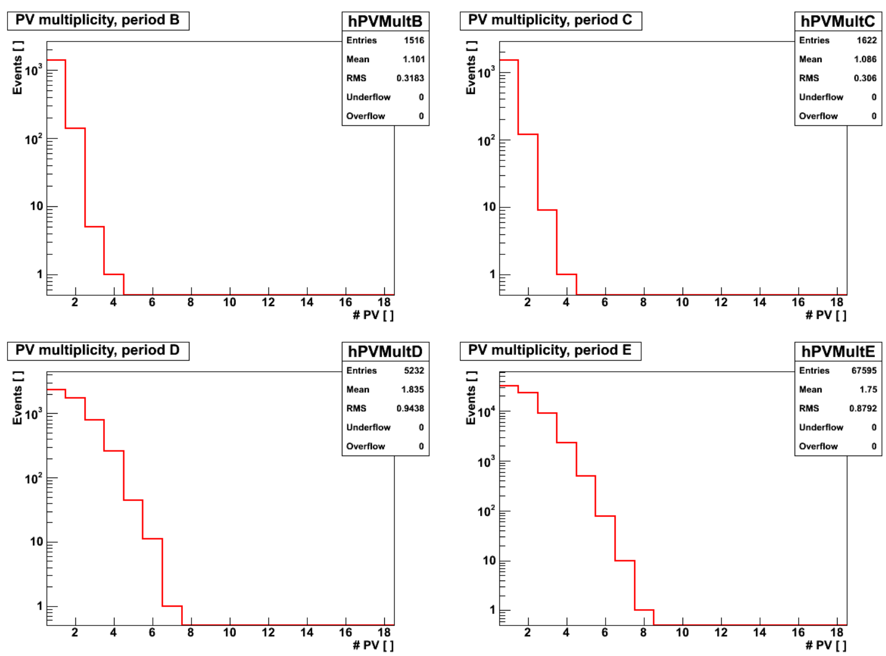


Figure B.1: Primary vertex multiplicity for periods B-E.

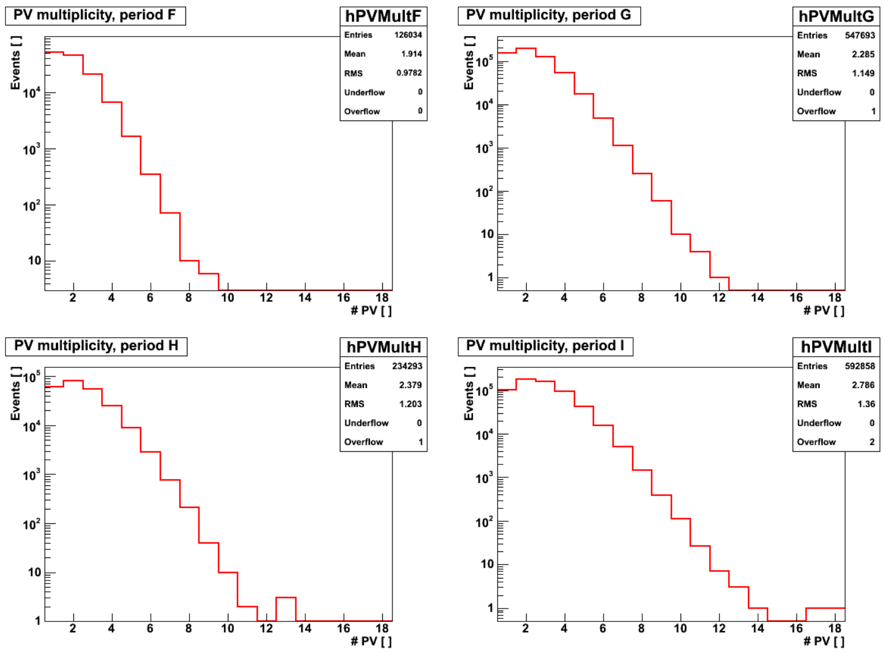


Figure B.2: Primary vertex multiplicity for periods F-I.

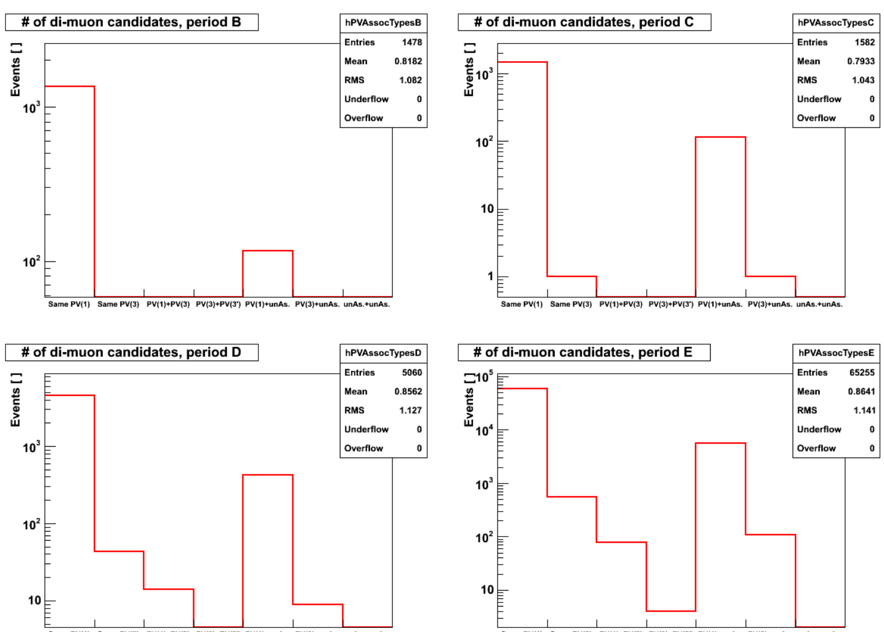


Figure B.3: Number of $J/\psi$ candidates (di-muons) for various primary vertices combinations (see 4.4) for periods B-E.

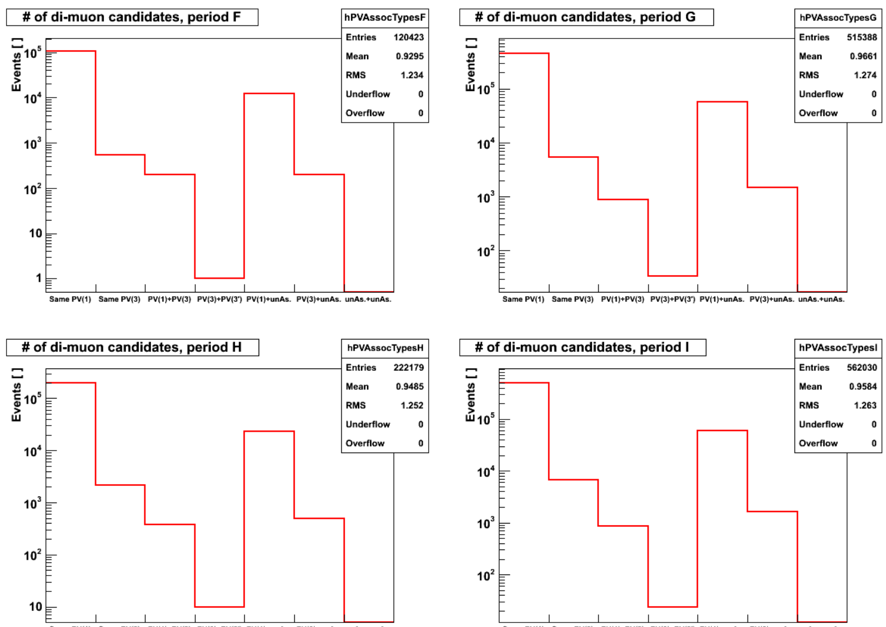


Figure B.4: Number of $J/\psi$ candidates (di-muons) for various primary vertices combinations (see 4.4) for periods F-I.

# Bibliography


[1] K. Nakamura *et al.* (Particle Data Group), J. Phys. G 37, 075021 (2010), available on the PDG web pages: `http://pdg.lbl.gov/`

[2] D. H. Perkins, *Introduction to High Energy Physics*, Cambridge University Press, UK, 2000

[3] J. H. Schwarz, *The Second Superstring Revolution*, `http://www.theory.caltech.edu/people/jhs/strings/index.html`

[4] Y. Fukuda *et al.* (The Super-Kamiokande Collaboration), *Measurements of the Solar Neutrino Flux from Super-Kamiokande's First 300 Days*, hep-ex/9805021v3, 1998

[5] M. Neubert, *Introduction to B Physics*, hep-ph/0001334v1, 2000

[6] T. Nakada, *B Physics at LHC(b)*, 2002, available from: `http://lphe.epfl.ch/publications/2002/iphe_02_003.pdf`

[7] LHC machine outreach website, `http://lhc-machine-outreach.web.cern.ch/lhc-machine-outreach`

[8] CERN FAQ - LHC the guide, available from: `http://cdsweb.cern.ch/record/1092437/files/CERN-Brochure-2008-001-Eng.pdf`

[9] ATLAS experiment public pages, `http://atlas.ch`

[10] ATLAS HLT/DAQ/DCS Group, *ATLAS High-Level Trigger, Data Acquisition and Controls Technical Design Report*, CERN, 2003, available from: `http://cdsweb.cern.ch/record/616089/files/cer-002375189.pdf`

[11] ATLAS Collaboration, *ATLAS Detector and Physics Performance Technical Design Report*, CERN, 1999, available from: `http://www.cern.ch/Atlas/GROUPS/PHYSICS/TDR/physics_tdr/printout/Volume_I.pdf`

[12] ATLAS Collaboration, *Expected Performance of the ATLAS Experiment: Detector, Trigger and Physics*, CERN, 2008, available from: `http://cdsweb.cern.ch/record/1125884/files/CERN-OPEN-2008-020.pdf`

[13] ATLAS Twiki pages - Trk::Perigee Class Reference, http://atlas-computing.web.cern.ch/atlas-computing/links/nightlyDevDirectory/AtlasOffline/latest_doxygen/InstallArea/doc//TrkParameters/html//classTrk_1_1Perigee.html

[14] ATLAS Twiki pages - InDet Tracking Performance Plots from the CSC Book, https://twiki.cern.ch/twiki/bin/view/Atlas/InDetTrackingPerformanceCSCFigures

[15] S. Hassini *et al.*, NIM A572 (2007) 77–79

[16] Th. Lagouri *et al.*, IEEE Trans. Nucl. Sci. 51 (2004) 3030–3033

[17] NYU participation in ATLAS, http://www.physics.nyu.edu/experimentalparticle/atlas.html

[18] ATLAS Twiki pages - The ATLAS Computing Workbook, https://twiki.cern.ch/twiki/bin/view/Atlas/WorkBook

[19] ATLAS Computing Group, *ATLAS Computing Technical Design Report*, CERN, 2005, available from: http://atlas-proj-computing-tdr.web.cern.ch/atlas-proj-computing-tdr/PDF/Computing-TDR-final-July04.pdf

[20] ROOT HomePage, http://root.cern.ch/

[21] RooFit HomePage, http://roofit.sourceforge.net/

[22] ROOT HomePage (RooFit), http://root.cern.ch/drupal/content/roofit

[23] ATLAS Collaboration, *Virtual Point 1*, http://atlas-vp1.web.cern.ch/atlas-vp1/

[24] ATLAS Collaboration, *Atlantis Event Display*, http://www.hep.ucl.ac.uk/atlas/atlantis/

[25] T. Jakoubek, *First look at multiple PV in di-muon, $J/\psi$ events*, Weekly BJpsi subgroup meeting, August 5, 2010, http://indico.cern.ch/contributionDisplay.py?contribId=4&confId=103187

[26] T. Jakoubek, *Multiple PV vertices and $J/\psi$ signal*, Weekly BJpsi meeting, August 19, 2010, http://indico.cern.ch/contributionDisplay.py?contribId=3&confId=104458

[27] T. Jakoubek, *$J/\psi$ mass wrt trigger*, Bd JpsiK0* signal meeting, October 25, 2010, http://indico.cern.ch/contributionDisplay.py?contribId=1&confId=111403

[28] T. Jakoubek, *Physics properties of $J/\psi$ events in testing of ID performance*, ATLAS seminar at IoP, November 12, 2010, http://www-hep2.fzu.cz/twiki/pub/ATLAS/AtlasSeminars/Jakoubek_JPsi_121110.pdf

[29] T. Jakoubek, *PV studies with $J/\psi \to \mu\mu$*, Weekly BJpsi meeting, November 17, 2010, http://indico.cern.ch/contributionDisplay.py?contribId=2&confId=113563

[30] ATLAS Collaboration, *Observation of the $B^{\pm} \to J/\psi(\mu^+\mu^-)K^{\pm}$ resonance in ATLAS*, CERN, 2010, available from: http://cdsweb.cern.ch/record/1293123/

[31] ATLAS $B$-physics group, *Analysis tools for B-physics*, https://twiki.cern.ch/twiki/bin/view/AtlasProtected/BPhysWorkingGroupAnalysisAndVertexing

[32] ATLAS Data Periods, https://twiki.cern.ch/twiki/bin/view/AtlasProtected/DataPeriods

[33] ATLAS Data Summary 2010, https://atlas.web.cern.ch/Atlas/GROUPS/DATAPREPARATION/DataSummary/2010/

[34] ATLAS Data Preparation - Reprocessing, https://twiki.cern.ch/twiki/bin/viewauth/Atlas/DataPreparationReprocessing

[35] ATLAS Collaboration, *$J/\psi$ Performance of the ATLAS Inner Detector*, CERN, 2010, available from: http://cdsweb.cern.ch/record/1281369/files/ATLAS-CONF-2010-078.pdf

[36] ATLAS Collaboration, *Performance of primary vertex reconstruction in proton-proton collisions at $\sqrt{s} = 7$ TeV in the ATLAS experiment*, CERN, 2010, available from: http://cdsweb.cern.ch/record/1281344/files/ATLAS-CONF-2010-069.pdf